Year: 2012

The Corepressor NCoR1 Antagonizes PGC-1α and Estrogen-Related Receptor α in the Regulation of Skeletal Muscle Function and Oxidative Metabolism

Pérez-Schindler, Joaquín and Summermatter, Serge and Salatino, Silvia and Zorzato, Francesco and Beer, Markus and Balwierz, Piotr J. and van Nimwegen, Erik and Feige, Jérôme N. and Auwerx, Johan and Handschin, Christoph

Originally published as:

Pérez-Schindler, Joaquín and Summermatter, Serge and Salatino, Silvia and Zorzato, Francesco and Beer, Markus and Balwierz, Piotr J. and van Nimwegen, Erik and Feige, Jérôme N. and Auwerx, Johan and Handschin, Christoph. (2012) *The Corepressor NCoR1 Antagonizes PGC-1α and Estrogen-Related Receptor α in the Regulation of Skeletal Muscle Function and Oxidative Metabolism.* Molecular and cellular biology, Vol. 32, H. 24. S. 4913-4924.

The Corepressor NCoR1 Antagonizes PGC-1α and ERRα in the Regulation of Skeletal Muscle Function and Oxidative Metabolism

Joaquín Pérez-Schindler,[a] Serge Summermatter,[a] Silvia Salatino,[a] Francesco Zorzato,[b,c] Markus Beer,[a] Piotr J. Balwierz,[a,d] Erik van Nimwegen,[a,d], Jérôme N. Feige,[e,f] Johan Auwerx,[f] and Christoph Handschin[a,#]

Biozentrum, University of Basel, Klingelbergstrasse 50/70, 4056 Basel, Switzerland[a]; Departments of Anesthesia and Biomedicine, Basel University Hospital, Hebelstrasse 20, CH-4031 Basel, Switzerland[b]; Department of Experimental and Diagnostic Medicine, University of Ferrara, Via Borsari 46, 44100 Ferrara, Italy[c]; Swiss Institute of Bioinformatics, Klingelbergstrasse 50/70, 4056 Basel, Switzerland[d]; Novartis Institute for Biomedical Research, 4056 Basel, Switzerland[e]; and Laboratory for Integrative and Systems Physiology, Ecole Polytechnique Fédérale de Lausanne, 1015 Lausanne, Switzerland[f]

Published in Mol Cell Biol. 2012 Dec;32(24):4913-24. PMID: 23028049. doi: 10.1128/MCB.00877-12

The Corepressor NCoR1 Antagonizes PGC-1α and ERRα in the Regulation of Skeletal Muscle Function and Oxidative Metabolism

Joaquín Pérez-Schindler,[a] Serge Summermatter,[a] Silvia Salatino,[a] Francesco Zorzato,[b,c] Markus Beer,[a] Piotr J. Balwierz,[a,d] Erik van Nimwegen,[a,d], Jérôme N. Feige,[e,f] Johan Auwerx,[f] and Christoph Handschin[a,#]

Biozentrum, University of Basel, Klingelbergstrasse 50/70, 4056 Basel, Switzerland[a]; Departments of Anesthesia and Biomedicine, Basel University Hospital, Hebelstrasse 20, CH-4031 Basel, Switzerland[b]; Department of Experimental and Diagnostic Medicine, University of Ferrara, Via Borsari 46, 44100 Ferrara, Italy[c]; Swiss Institute of Bioinformatics, Klingelbergstrasse 50/70, 4056 Basel, Switzerland[d]; Novartis Institute for Biomedical Research, 4056 Basel, Switzerland[e]; and Laboratory for Integrative and Systems Physiology, Ecole Polytechnique Fédérale de Lausanne, 1015 Lausanne, Switzerland[f]

[#]Address correspondence to Christoph Handschin, christoph.handschin@unibas.ch.

Running title: Regulation of skeletal muscle function by NCoR1

Word count for the Materials and Methods: 1767 words.

Word count for the introduction, Results, and Discussion: 3890 words.

Keywords: muscle remodeling; muscle metabolism; NCoR1; PPARβ/δ; ERRα; PGC-1α

Abstract

Skeletal muscle exhibits a high plasticity and accordingly can quickly adapt to different physiological and pathological stimuli by changing its phenotype largely through diverse epigenetic mechanisms. The nuclear receptor corepressor 1 (NCoR1) has the ability to mediate gene repression; its role in regulating biological programs in skeletal muscle however is still poorly understood. We therefore studied the mechanistic and functional aspects of NCoR1 function in this tissue. NCoR1 muscle-specific knockout mice exhibited a 7.2% higher VO_{2peak}, a 11% reduction in maximal isometric force and increased ex vivo fatigue resistance during maximal stimulation. Interestingly, global gene expression analysis revealed a high overlap between the effects of NCoR1 deletion and peroxisome proliferator-activated receptor (PPAR) γ coactivator 1α (PGC-1α) overexpression on oxidative metabolism in muscle. Importantly, PPARβ/δ and estrogen-related receptor α (ERRα) were identified as common targets of NCoR1 and PGC-1α with opposing effects on the transcriptional activity of these nuclear receptors. In fact, the repressive effect of NCoR1 on oxidative phosphorylation gene expression specifically antagonizes PGC-1α-mediated coactivation of ERRα. We therefore delineated the molecular mechanism by which a transcriptional network controlled by corepressor and coactivator proteins determines the metabolic properties of skeletal muscle, thus representing a potential therapeutic target for metabolic diseases.

Introduction

An improved muscle performance is directly linked to a lower prevalence of metabolic diseases (9, 50). In fact, while physical exercise and training can lower morbidity and mortality, physical inactivity has been recognized as one of the main risk factors for these pathologies (8). Lower whole body aerobic capacity, muscle mitochondrial content and oxidative activity, which all correlate with a sedentary life-style, contribute to the development of metabolic disorders (9, 25, 34, 38). Therefore, maintenance or improvement of skeletal muscle function, especially its oxidative metabolism, should be considered among the first interventions in the treatment and prevention of metabolic diseases.

Skeletal muscle is a highly plastic tissue that can quickly adapt to different physiological (e.g. exercise) and pathological (e.g. over-nutrition) stimuli. In fact, muscle fibers can change their gene expression profile and phenotype to a great extent through diverse epigenetic mechanisms (3, 6, 31). Accordingly, muscle remodeling is highly regulated by different transcription factors and coregulator complexes, which are able to modify chromatin structure and thereby regulate gene transcription (27, 41). The nuclear receptor corepressor 1 (NCoR1) is a ubiquitously expressed corepressor, originally identified as the mediator of ligand-independent transcriptional repression of the thyroid hormone and the retinoic acid receptor (22). NCoR1 interacts with several transcription factors through its receptor interaction domains located in the C-terminus (48). However, because NCoR1 lacks intrinsic histone deacetylase (HDAC) activity, it regulates gene transcription by forming a large protein complex, in which G-protein-pathway suppressor 2 (GPS2), transducin β-like 1 (TBL1), TBL-related 1 (TBLR1) and HDAC3 represent the core subunits (52). In fact, the

NCoR1-HDAC3 interaction plays an essential role in the control of gene transcription, since HDAC3 is directly activated by the deacetylase activation domain (DAD) of NCoR1 (23).

NCoR1 interacts with different proteins that play an important role in muscle physiology, such as peroxisome proliferator-activated receptors (PPAR) and p85α (15, 32), though its role in skeletal muscle remains largely enigmatic. Cell culture experiments implied that NCoR1 modulates myoblast differentiation through the regulation of the expression and transcriptional activity of several transcription factors, e.g. MyoD, TRα1 and Csl (5, 10, 26). The role of NCoR1 in vivo is not well understood because *Ncor1*$^{-/-}$ mice embryos die during gestation (24). Recently, conditional knockout models revealed that NCoR1 is an important player of skeletal muscle and adipose tissue energy metabolism (28, 51). In skeletal muscle, NCoR1 deletion enhances oxidative metabolism and slightly improves insulin tolerance under high fat diet (51). Specific genetic ablation of NCoR1 in white adipose tissue lowers inflammation and improves whole body insulin sensitivity (28). However, the mechanism by which NCoR1 deletion result in these effects is not well understood.

NCoR1 is expressed in adult glycolytic and oxidative muscles at equal levels (42, 43). Chronic low frequency stimulation of rat hindlimb and acute endurance exercise in mice repress the expression of NCoR1 in this tissue (42, 51). Interestingly, by using knockout mice, it has been demonstrated that the formation of slow oxidative muscle fibers is negatively regulated by class IIa HDACs (39), which depend on interaction with the NCoR1-HDAC3 complex in order to induce protein deacetylation (14). Consistently, the global disruption of the NCoR1-HDAC3 complex in mice results in an improved energy metabolism (e.g. higher insulin sensitivity and oxygen consumption) and altered circadian behavior (2). The aim of this study was to further investigate the role of NCoR1 in different aspects of skeletal muscle

function (e.g. force generation) and, importantly, to elucidate the elusive mechanism by which NCoR1 regulates oxidative metabolism in this tissue.

MATERIAL AND METHODS

Animals housing and NCoR1 MKO mice generation. Mice were housed in a conventional facility with a 12 h night and day cycle, with free access to food and water. All experiments were performed on adult male mice with approval of the Swiss authorities. NCoR1 MKO animals were generated as previously described (51). Briefly, *Ncor1*$^{loxP/loxP}$ mice were crossed with *HSA*-*Cre* transgenic mice to generate NCoR1 MKO mice. *Ncor1*$^{loxP/loxP}$ animals without *Cre* expression were used as control (CON) mice. No overt phenotypic differences between CON and wild type mice were observed. Genotyping was performed from tail biopsies by PCR using specific primer pairs to detect the presence of the 5' and 3' loxP sites. The presence of the 5' loxP site resulted in an amplicon of 450 bp (wild type (WT) allele 403 bp), while the presence of the 3' loxP site resulted in an amplicon of 346 bp (WT allele 207 bp) (Fig. S1A). Specific primer pairs to detect *Cre* recombinase resulted in an amplicon of 320 bp in NCoR1 MKO animals (Fig. S1A). In addition, using muscle samples, recombination was confirmed by PCR using the forward and reverse primers used to detect the 5' and 3' loxP sites, respectively. Consequently, a 246 bp band was detected exclusively in NCoR1 MKO animals (Fig. S1B). The recombination of the *Ncor1* floxed allele decreased its mRNA specifically in skeletal and, to a smaller extent, in cardiac muscle compared to CON mice (Fig. S1C). Importantly, previous work has indicated that the slight decrease of NCoR1 mRNA in the heart of MKO mice does not affect cardiac morphology and function (51).

The generation and characterization of transgenic mice expressing PPARγ coactivator 1 (PGC-1) α under the control of the MCK promoter has been published (30). These PGC-1α

mTg mice exhibit a 9.5 fold increase in skeletal muscle PGC-1α mRNA (Fig. S3A), higher oxidative metabolism and improved exercise performance (11, 30).

Exercise performance assessment. Animals were acclimatized to treadmill running for two days. On the first day, mice ran in a closed treadmill (Columbus Instruments) for 5 min at 10 m/min with a 0° slope, followed by 5 min at 14 m/min with a 5° incline. On the second day, animals ran for 5 min at 10 m/min with a 5° incline, followed by 5 min at 14 m/min. To determine maximal exercise performance and VO_{2peak}, indirect calorimetry was performed during a maximal exercise test. Thus, two days after the acclimatization, mice were placed in a closed treadmill for 6 min at 0 m/min with a 5° incline. Subsequently, the test started at 8 m/min for 3 min with a 5° incline and the speed increased 2 m/min every 3 min until exhaustion.

To determine endurance performance, mice were placed in an open treadmill (Columbus Instruments) for 5 min at 0 m/min with a 5° incline, followed by 5 min at 8 m/min. Then, mice ran for 20 min at 60, 70, 80 and 90% of the maximal speed reached in the maximal exercise test (average of the group), then the speed increased to 100% of the maximal speed until exhaustion. The endurance test was performed at least three days after the maximal test.

Blood lactate analysis. Blood lactate was measured from the tail vein of overnight fasted (16 h) mice or fed animals before and after different time point after treadmill running (see maximal exercise test) using a lactate meter (Nova Biomedical).

In vivo measurement of muscle contractility. Grip strength of the fore- and hindlimbs was measured with a grip strength meter (Chatillon). To determine the maximal strength, three measurements were performed with at least 60 s of recovery between each repetition, and the maximum value obtained was used for the analysis. To assess isometric fatigue resistance, mice were placed on top of an elevated grid and the maximum time that they could remain on the inverted grid was recorded.

Ex vivo determination of muscle contractility. Maximal force and fatigue resistance of extensor digitorum longus (EDL) and soleus were measured with a muscle testing setup (Heidelberg Scientific Instruments). Contraction amplitude was digitalized at 4 kHz with an AD Instruments converter. After the determination of the optimal length, force generation of EDL and soleus during a single twitch was measured in response to 15 V pulse for 0.5 ms. Tetanic contraction was assessed in response to 15 V pulse at 150 Hz for 400 ms for EDL and 1,100 ms for soleus. Maximal force and kinetics of the single twitch and tetanus were recorded and analyzed.

After 10 min of recovery following the tetanic stimulation, fatigue resistance of EDL and soleus was assessed under two different protocols. First, a long interval protocol was performed by stimulating the muscles with a 15 V pulse at 150 Hz for 350 ms at 3.6 s interval during 6 min for EDL and 10 min for soleus, followed by 10 min recovery. Subsequently, a short interval protocol was performed by stimulating the muscles with a 15 V pulse at 150 Hz for 350 ms at 1 s interval during 2 min for EDL and 3 min for soleus. Changes in force generation are expressed as percentage of initial force (first tetanus) (18).

Cell culture experiments. C_2C_{12} myoblasts were grown in Dulbecco's Modified Eagle's Medium (DMEM) supplemented with 10% fetal bovine serum and 1% penicillin/streptomycin (growth medium). To induce differentiation, growth media of 90-95% confluent myoblasts was changed to DMEM supplemented with 2% horse serum and 1% penicillin/streptomycin (differentiation medium). Cells were maintained at 37°C, 95% O_2 and 5% CO_2.

Experiments using C_2C_{12} cells were performed on fully differentiated myotubes 4 days after differentiation was induced. For knockdown experiments, different adenoviruses containing specific shRNAs against NCoR1, PGC-1α, PGC-1β and LacZ (control) were used. Cells were incubated with the corresponding adenovirus for 24 h, and then adenovirus containing-medium was changed for fresh differentiation medium for another 24 h. In addition, cells were treated for 48 h with 0.2% DMSO (as control), 10 µM XCT790 (Sigma-Aldrich) to inhibit ERRα or 1 µM GSK0660 (Sigma-Aldrich) to inhibit PPARβ/δ, together with the corresponding adenovirus. Three independent experiments were performed in triplicate each.

Luciferase assay were performed on 12 well plate using COS-7 cells (African green monkey kidney fibroblast-like cells) grown in growth medium without antibiotics. COS-7 cells were used in our experiments as a heterologous experimental system and furthermore, because of their high transfection efficiency and suitability for expressing constructs containing SV40 promoters. Cells were transfected using Lipofectamine^{TM} 2000 (Invitrogen) with 0.1 µg pRL-SV40 (Promega: E2231), 0.3 µg pPPRE X3-TK-luc (Addgene: 1015; Bruce Spiegelman), 0.3 µg pERRE-luc (gift of Dr. Junichi Sadoshima) (36), 0.4 µg pBABE puro PPAR delta (Addgene: 8891; Bruce Spiegelman), 0.4 µg pERRα (gift of Dr. Vincent Giguère), 0.4 µg pFlag-NCoR (gift of Dr. Christopher K. Glass), 0.4 µg pAd-Track HA PGC-1 alpha (Addgene: 14427; Pere

Puigserver). Total amount of plasmid DNA was kept constant at 1.6 µg per well by using the control plasmid pAdtrack-CMV (ATCC). Twenty four hours after transfection cells were lysed with 250 µL of 1X Passive Lysis 5X Buffer (Promega) and luciferase activity was measured in 75 µL of lysate in a 96 well plate using the Dual-Glo® Luciferase Assay System (Promega). Renilla (pRL-SV40) luciferase activity was used for normalization. Five independent experiments were performed in triplicate each.

RNA isolation and real-time PCR. Total RNA was isolated from C_2C_{12} myotubes, liver, kidney, white adipose tissue, heart, gastrocnemius, soleus, plantaris, tibialis anterior, extensor digitorum longus and quadriceps from NCoR1 MKO mice or gastrocnemius from PGC-1α mTg animals using lysing matrix tubes (MP Biomedicals) and TRI Reagent® (Sigma-Aldrich) according to the manufacturer's instructions. RNA concentration was measured with a NanoDrop 1000 spectrophotometer (Thermo Scientific). One microgram of RNA was treated with DNase I (Invitrogen) and then reversed transcribed using hexanucleotide mix (Roche) and SuperScript™ II reverse transcriptase (Invitrogen). Relative mRNA was quantified by Real-Time PCR on a StepOnePlus system (Applied Biosystems) using Power SYBR® Green PCR Master Mix (Applied Biosystems). The analysis of the mRNA was performed by the $\Delta\Delta C_T$ method using TATA binding protein (TBP) as endogenous control. Primers used for target genes and TBP had the same PCR efficiency. TBP transcript levels were not different between genotypes or different experimental conditions. Primers sequence can be found in Supplemental Table 3.

Mitochondrial DNA measurement. DNA was isolated from gastrocnemius using NucleoSpin® Tissue kit (Macherey-Nagel). Real-time PCR analysis was performed to measure COX2 (mitochondrial DNA) and β-globin (nuclear DNA) levels.

Skeletal muscle staining. Oxidative fibers were detected by NADH staining of 12 µm cross sections from tibialis anterior. Staining was performed by exposing the sections to 0.8 mg/mL NADH in the presence of 1 mg/mL Nitro-blue tetrazodium. Periodic Acid-Schiff (PAS) staining was performed with a PAS Kit following the manufacture's instructions (Sigma-Aldrich).

Protein isolation. Tissue samples were powdered on dry ice and homogenized with a polytron in 300 µL of ice-cold lysis buffer (50 mM Tris-HCl pH 7.5, 250 mM Sucrose, 1 mM EDTA, 1 mM EGTA, 0.25% Nonidet P 40 substitute, 50 mM NaF, 5 mM $Na_4P_2O_7$, 0.1% DTT, fresh protease and phosphatase inhibitor cocktail). Then, samples were shaken at 1,300 rpm for 30 min at 4°C. Samples were subsequently centrifuged at 13,000 g for 10 min at 4°C and the protein concentration of the supernatant determined by the Bradford assay (Bio-Rad). Equal aliquots of protein were boiled for 5 min in Laemmli sample buffer (250 mM Tris-HCl pH 6.8, 2% SDS, 10% glycerol, 0.01% bromophenol blue and 5% β-mercaptoetanol).

Western blot. Samples were separated on SDS-polyacrylamide gels and then transferred to nitrocellulose membranes for 60 min. Membranes were blocked for 1 h in 3% milk, Tris-buffered saline and 0.1% tween-20 (TBST) before overnight incubation at 4°C with appropriate primary antibody in TBST (1:1,000 dilution). Proteins were detected with a

primary antibody to p-AMPKα^{T172} (Cell Signaling: 2535) and AMPKα (Cell Signaling: 2603). As loading control, eEF2 (Cell Signaling: 2332) was used. Following incubation, membranes were washed 3 times with TBST before incubation with an appropriate peroxidase-conjugated secondary antibody in TBST (1:10,000 dilution). Antibody binding was detected using enhanced chemiluminescence HRP substrate detection kit (Pierce: 32106).

Microarray and bioinformatic analysis. RNA from gastrocnemius was isolated with miRNeasy Mini Kit (QIAGEN) and microarray was performed using the GeneChip® Gene 1.0 ST Array System (Affymetrix). In addition, Gene Ontology analysis was performed us the online tool FatiGO (http://babelomics.bioinfo.cipf.es/index.html) (1). Finally, microarray data was analyzed using Motif Activity Response Analysis (http://www.mara.unibas.ch/cgi/mara) (47).

Statistical analysis. Values are expressed as mean ± standard error of the mean (SEM). Statistical significance was determined with unpaired two-tailed t-tests or one-way ANOVA with Tukey's post-hoc test. Significance was considered with a $p < 0.05$.

Accession Number

Microarray data can be found at Gene Expression Omnibus (GEO) under accession number GSE40439.

RESULTS

Muscle NCoR1 deletion enhances VO_2 during maximal exercise and decreases muscle contractility. The role of NCoR1 in skeletal muscle was studied using NCoR1 muscle-specific knockout (NCoR1 MKO) mice. A full description of this animal model has been recently published elsewhere (51). First, we assessed maximal oxidative capacity and treadmill running performance. Both genotypes exhibited the same exercise performance during a maximal and endurance exercise tests, as reflected by equal speed, distance, time, work and power (Table S1). However, NCoR1 MKO mice reached a significantly higher (7.2%) VO_{2peak} during the maximal exercise test (CON 125 ± 1.2 mL/kg/min vs. MKO 134 ± 1.5 mL/kg/min, $p < 0.001$). In fact, NCoR1 MKO animals showed a higher VO_2 at 50, 80, 90 and 100% of maximal speed (Fig. 1A). Blood lactate measurement before and after maximal exercise, or during fasting, was not different in NCoR1 MKO mice (Fig. S2A and B). Consistently, RER measurement during the maximal exercise test did not show differences between CON and NCoR1 MKO mice (Fig. S2C), indicating that energy substrate utilization was not altered by NCoR1 deletion. We then performed NADH and PAS staining of skeletal muscle to determine the proportion of oxidative fibers and glycogen content, respectively. NCoR1 MKO animals showed a 10% increase in oxidative fibers compared to CON mice (Fig. 1B), but glycogen content was not significantly affected (Fig. 1C). Furthermore, we have found higher levels of AMP-activated protein kinase (AMPK) phosphorylation in skeletal muscle of NCoR1 MKO mice (Fig. 1D). Altogether, these data show that NCoR1 deletion in striated muscle results in an enhanced oxidative metabolism, in particular during high-intensity exercise.

An important aspect of muscle function besides endurance is the ability to generate force. To assess muscle contractility in vivo, we measured maximal grip strength of the fore- and

hindlimbs. We observed a trend for lower peak isometric force generated by the forelimbs (p = 0.078) and a significant reduction by 11% in the hindlimbs of NCoR1 MKO animals (Fig. 1E). Then, we quantified muscle fatigue resistance during predominantly isometric muscle contraction by measuring the maximal time that mice could remain on an inverted grid. Consistent with the lower maximal isometric force, isometric fatigue resistance was also decreased in NCoR1 MKO animals (Fig. 1F). To exclude systemic and neural factors that could affect force generation in vivo, we also determined muscle contractility in isolated muscles. Absolute (p < 0.05) and specific (p = 0.056) muscle contractility in response to a single twitch was decreased in the glycolytic muscle extensor digitorum longus (EDL), but not in the oxidative muscle soleus (Fig. 2A and B). Conversely, when EDL and soleus were subjected to maximal tetanic stimulation, no differences between genotypes were observed (Fig. 2C and D). Moreover, the contractile kinetics of EDL and soleus in response to a single twitch or a maximal tetanic stimulation were not significantly different between CON and NCoR1 MKO mice (Table S1).

Finally, muscle fatigue resistance was determined ex vivo by a long and short interval protocol. As expected, soleus exhibited a lower decrease in force than EDL in the long interval protocol, but no differences between genotypes were found (Fig. 2E). Similarly, soleus had a higher fatigue resistance than EDL during the short interval protocol. However, in this protocol, EDL from NCoR1 MKO animals exhibited a lower decrease in force generation, while soleus of NCoR1 MKO and CON mice were identical (Fig. 2F). In fact, in the short interval protocol, EDL from NCoR1 MKO mice generated ~43% more force from the tetanus 35 to 100 (see inset Fig. 2F) indicating a higher muscle fatigue resistance. Therefore, it seems that glycolytic muscles are more susceptible to the effect of NCoR1 deletion on

muscle contractility, resulting in a decreased maximal isometric force and increased fatigue resistance during maximal stimulation.

NCoR1 and PGC-1α target a common subset of genes involved in oxidative metabolism. The phenotype exhibited by NCoR1 MKO animals implies a direct link between NCoR1 and oxidative metabolism. At the transcriptional level, mitochondrial function is mainly regulated by the PPARγ coactivator 1 (PGC-1) family of coactivators, which are able to activate different transcription factors such as ERRα and NRF-1 (29). Interestingly, NCoR1 MKO mice mirror some aspects of the phenotype exhibited by PGC-1α muscle-specific transgenic (mTg) mice, such as the enhanced oxidative metabolism and decreased maximal force (11, 30, 45). To explore the idea of an NCoR1-PGC-1α crosstalk and to further characterize the oxidative phenotype of NCoR1 MKO mice, microarray analyses of gene expression patterns in NCoR1 MKO and PGC-1α mTg skeletal muscles were compared. Gene Ontology (GO) enrichment analysis revealed over-representation of transcripts related to metabolic pathways such as “oxidative phosphorylation” and “citrate cycle (TCA cycle)” in both NCoR1 MKO and PGC-1α mTg animals (Fig. 3A, B and Fig. S4A to F). Interestingly, when both microarray data sets were compared, we observed that 188 of the genes affected by NCoR1 deletion were also found in the PGC-1α mTg data set, suggesting that ~50% of the genes regulated by NCoR1 are also targets of PGC-1α (Fig. 3C). When only the genes found in the GO terms “oxidative phosphorylation” and “citrate cycle (TCA cycle)” where compared, we found that all of the genes present in NCoR1 MKO data set were also targets of PGC-1α (Fig. 3C). Interestingly, we observed that in both microarrays all of these common genes were actually up-regulated (Fig. 3D and E). Several of these transcripts were validated by real-time PCR analysis of GAS, EDL and soleus (Fig. S3B and C), confirming the results

obtained in the microarrays. However, no fiber type-specific (oxidative vs. glycolytic) differences in terms of regulation of gene expression were observed in NCoR1 MKO mice (Fig. S3C). Furthermore, skeletal muscle from NCoR1 MKO and PGC-1α mTg mice had higher transcript levels of mitochondrial encoded genes involved in oxidative metabolism, such as cytochrome c oxidase subunit I (*COX1*), ATP synthase F0 subunit 6 (*ATP6*) and NADH dehydrogenase subunit 1 (*ND1*) (Fig. 3F and Fig. S3B). However, no differences in transcription factor A, mitochondrial (*TFAM*) mRNA levels and mitochondrial DNA content was found as a consequence of NCoR1 deletion (Fig. 3G and 6A). These results further demonstrate the role of NCoR1 in the transcriptional control of different mitochondrial pathways and strongly suggest a role of PGC-1α in the control of the oxidative phenotype of the NCoR1 MKO animals.

Interestingly, the mRNA level of PGC-1α was not different in NCoR1 MKO compared to CON mice (Fig. 4A and Fig. S5A). In contrast, we found an increase in PGC-1β and a slight decrease in PGC-1-related coactivator (PRC) transcript levels in gastrocnemius and soleus from NCoR1 MKO mice (Fig. 4A and Fig. S5A). To dissect the contribution of the PGC-1 family members to the effects induced by NCoR1 knockdown, we studied C_2C_{12} myotubes in culture that were virally transfected with two different shRNAs specifically targeting NCoR1 (Fig. 4B, Fig. S5B and C, Fig. S6A and B). Then, we selectively induced the knockdown of PGC-1α or PGC-1β with specific shRNA constructs (Fig. 4B and Fig. S5B). Similar to the NCoR1 MKO animals, NCoR1 knockdown in C_2C_{12} myotubes also induced an up-regulation of succinate dehydrogenase complex, subunit A, flavoprotein (*SDHa*), NADH dehydrogenase (ubiquinone) 1 α subcomplex 5 (*NDUFA5*), NADH dehydrogenase (ubiquinone) 1 β subcomplex 5 (*NDUFB5*) and fumarate hydratase 1 (*FH1*) (Fig. 4C), in addition to the

mitochondrial encoded genes *COX1* and *ATP6* (Fig. 4C). Surprisingly, NCoR1 knockdown in C_2C_{12} myotubes induced a big increase in PGC-1α mRNA (Fig. 4B). Importantly however, although the simultaneous knockdown of PGC-1α partially prevented its up-regulation, shRNA-mediated reduction of PGC-1α was sufficient to strongly inhibit the up-regulation of *SDHa*, *NDUFA5*, *NDUFB5*, *FH1*, *COX1* and *ATP6* mRNA induced by NCoR1 knockdown (Fig. 4C). In the cultured muscle cells, NCoR1 knockdown did not alter PGC-1β gene expression (Fig. S5B), while the opposite was observed in the NCoR1 MKO animals (Fig. 4A and Fig. S5A). In stark contrast to the knockdown of PGC-1α, the up-regulation of the nuclear and mitochondrial encoded genes induced by NCoR1 knockdown was not significantly affected by the simultaneous knockdown of PGC-1β in the cultured myotubes (Fig. 4D). Consistent with the microarray analysis, these results indicate that NCoR1 deletion enhance PGC-1α action on oxidative metabolism, probably due to a reduced competition between NCoR1 and PGC-1α for the regulation of common target genes.

NCoR1 and PGC-1α regulate oxidative metabolism through opposite modulation of ERRα. Our data suggest that NCoR1 and PGC-1α likely target the same subset of transcription factors involved in the regulation of oxidative metabolism with opposite effects on transcriptional activation. In order to elucidate potential common transcription factors of NCoR1 and PGC-1α in skeletal muscle, we performed Motif Activity Response Analysis (MARA) (47) of our microarray data to predict the core set of transcription factors which significantly change their activity in response to NCoR1 deletion or PGC-1α overexpression. Consistent with the oxidative phenotype of these two mouse models, retinoid X receptor (RXR) and estrogen-related receptor (ERR) α (also known as *Esrra*) were found among the top 4 most significant (z value ≥ 1.5) motifs (Fig. 5A, 5B and Table S2) and exhibited one of

the highest activity in response to NCoR1 deletion and PGC-1α overexpression (Fig. 5C to F). Given that RXRs are the main partners of PPARs (13), this suggests a possible PPARβ/δ activation in MKO animals. In fact, PPARβ/δ or ERRα in complex with PGC-1α and PGC-1β are known to be key players in the regulation of muscle metabolism (13, 16, 29). In contrast, the role of the transcription factors with significantly decreased activity (z value ≤ -1.5) in NCoR1 MKO and PGC-1α mTg mice (Fig. 5A, 5B and Table S2) is not well known. Similar to the microarray analysis, the comparison of both MARA analyses showed that 44% of the transcription factors found in NCoR1 MKO data set were also predicted in PGC-1α mTg MARA analysis, actually there is a larger overlap among motifs with increased activity (5 out of 9) than among ones with decreased activity (2 out of 7) (Fig. 5G). In summary, MARA-based biocomputational prediction strongly suggests ERRα and possibly the RXR-heterodimerization partner PPARβ/δ as common targets of NCoR1 and PGC-1α.

The mRNA levels of PPARβ/δ, ERRα and several transcription factors revealed by MARA were not increased in NCoR1 MKO mice (Fig 6A), indicating that increased activity is rather the consequence of a lower repression than of a higher expression. In order to explore the potential repressive effect of NCoR1 on ERRα and PPARβ/δ transcriptional activity, we transfected COS-7 cells with either a reporter plasmid containing PPAR response elements (PPRE-luc) or ERR response elements (ERRE-luc), together with expression plasmids for PPARβ/δ and ERRα, respectively. Next, we measured relative luciferase activity in the absence and presence of NCoR1 and PGC-1α. As predicted, NCoR1 decreased PPRE-luc and ERRE-luc luciferase activity by 43% and 36%, respectively (Fig. 6B and C). Inversely, PGC-1α induced a significant increase in PPRE-luc and ERRE-luc luciferase activity by 2037% and 161%, respectively (Fig. 6B and C). Importantly, we have found that the activation of both

PPRE-luc and ERRE-luc by PGC-1α was significantly decreased by NCoR1 (Fig. 6B and C). These data demonstrate that NCoR1 represses the transcriptional activity of both PPARβ/δ and ERRα, while PGC-1α competes with NCoR1 to exert a positive effect.

Finally, to study the relative contribution of PPARβ/δ and ERRα to the regulation of the oxidative phenotype exhibited in response to NCoR1 deletion in muscle, we used the PPARβ/δ selective antagonist GSK0660 (44) and the ERRα inverse agonist XCT790 (33, 49). As expected, GSK0660 induced a strong decrease in the mRNA level of the PPARβ/δ target gene uncoupling protein 3 (*UCP3*) (Fig. S6A) demonstrating the efficiency of the antagonist and the presence of functional PPARβ/δ in C_2C_{12} myotubes. Neither NCoR1 knockdown nor GSK0660 treatment changed *PPARβ/δ* mRNA levels (Fig. S6A). Importantly however, the induction of *SDHa*, *NDUFA5*, *NDUFB5*, *FH1*, *COX1* and *ATP6* mRNA were not inhibited by GSK0660 in cells with a knockdown of NCoR1 (Fig. 6D). Consistently, the mRNA levels of different PPARβ/δ target genes like carnitine palmitoyltransferase 1b (*CPT1b*), lipoprotein lipase (*LPL*) and *UCP3* were not significantly increased in NCoR1 MKO mice (Fig. S3C). In contrast, ERRα inhibition with XCT790 completely blocked the effects of NCoR1 knockdown on nuclear and mitochondrial encoded genes (Fig. 6E). However, different from the NCoR1 MKO animals, NCoR1 knockdown induced an up-regulation of *ERRα* in C_2C_{12} myotubes (Fig. S6B). This up-regulation of *ERRα* mRNA was only partially prevented by XCT790 (Fig. S6B), indicating that ERRα activation, rather than its up-regulation, is responsible for the effects of NCoR1 knockdown of oxidative metabolism in C_2C_{12} myotubes. Interestingly, similar to NCoR1 and PGC-1α microarray analysis, GO enrichment analysis of previously published ERRα ChIP-chip data from mouse liver (12) also revealed over-representation of transcripts related to “oxidative phosphorylation” (Fig. S4G). Furthermore, we found a high overlap

411 between the NCoR1 MKO microarray and the ERRα ChIP-chip data sets when comparing the
412 genes found in the GO term “oxidative phosphorylation” (Fig. S4H). Therefore, these data
413 suggest that ERRα and PGC-1α are essential for the effects of NCoR1 deletion on oxidative
414 metabolism in skeletal muscle, while PPARβ/δ and PGC-1β seems to play a minor role in this
415 experimental context.
416

DISCUSSION

In stark contrast to obese and type 2 diabetic subjects, endurance athletes exhibit an increased metabolic fitness and consequently lower risk for metabolic disorders (9, 35). Importantly, most of the adaptations to muscle use (e.g. endurance training) and disuse (e.g. physical inactivity) are under the coordinated control of different transcription factors and coregulators (7, 19). NCoR1 and its homolog NCoR2 have been recently suggested as important modulators of energy metabolism in several tissues, including skeletal muscle (28, 40, 46, 51). Consistently, we observed that NCoR1 MKO animals exhibit an increased VO_2 during high-intensity exercise. Surprisingly, while Yamamoto et al. (51) have reported an improved exercise performance in NCoR1 MKO mice, we did not observed significant differences in distance, time or work in the exercise trial in our experimental context. Considering the mild effect of NCoR1 deletion on muscle oxidative metabolism, it is possible that small differences in the exercise test protocol could significantly affect exercise performance. In addition, as previously shown (51), we observed a higher proportion of oxidative fibers in NCoR1 MKO skeletal muscle. Interestingly, our data also indicate a higher activation of AMPK in NCoR1 MKO mice, which has been associated with enhanced oxidative metabolism (20, 21). Importantly, we have now demonstrated that NCoR1 control skeletal muscle oxidative metabolism primarily through the regulation of ERRα and PGC-1α. NCoR1 deletion in striated muscle led to an increase in the mRNA content of a broad range of mitochondrial enzymes, thus supporting its potential role as negative regulator of oxidative metabolism. In agreement with this idea, NCoR1 MKO mice recapitulate many aspects of the phenotype exhibited by PGC-1α mTg mice, such as the increased expression of mitochondrial enzymes, higher levels of oxidative fibers and enhanced VO_{2peak} during

maximal exercise (11, 30, 51). Moreover, as found in NCoR1 MKO animals, PGC-1α overexpression in skeletal muscle also results in a reduced maximal force and increased muscle fatigue resistance (30, 45). Curiously, only EDL exhibited a higher muscle fatigue resistance during the short interval protocol in NCoR1 MKO mice. Since EDL is a highly glycolytic muscle, it might be more susceptible to benefit from the mild improvement on oxidative metabolism as consequence of NCoR1 deletion compared to the predominantly oxidative soleus. Analysis of NCoR1 MKO- and PGC-1α mTg-based microarrays also showed a high level of similarity between these mouse models, since all of the up-regulated genes related to oxidative metabolism found in NCoR1 MKO mice were also increased by PGC-1α overexpression. Hence, our findings indicate that NCoR1 deletion facilitates PGC-1α action on its target genes. In fact, PGC-1α mRNA was not increased in NCoR1 MKO mice, suggesting that the higher transcription of its target genes is not associated to its up-regulation. In contrast, NCoR1 knockdown in cultured cells induced a 133 fold increase in PGC-1α mRNA. Hence, it is possible that the bigger effects of NCoR1 deletion in C_2C_{12} myotubes compared to the mice are a consequence of both an up-regulation of PGC-1α and a lower competition between these coregulators. Importantly however, we found that knockdown of PGC-1α, but not PGC-1β, in C_2C_{12} myotubes completely blocked the effects of NCoR1 knockdown on oxidative metabolism, underlining the essential role of PGC-1α in this process. Similarly, prediction of the relative contribution of transcription factors to the gene expression pattern exhibited by NCoR1 MKO and PGC-1α mTg animals revealed a significant overlap between these mouse models. Interestingly, RXRs (heterodimerization partners for the PPARs) and ERRα stood out as top candidates, showing the strongest link to the control of energy metabolism (13, 16). In fact, Yamamoto et al. (51) have recently showed that in

463 C_2C_{12} myotubes, NCoR1 is recruited to the PPRE and nuclear receptor half-sites (ERR binding
464 site) of *UCP3* and *PDK4* promoter, respectively, though whether the effects of NCoR1
465 deletion on gene expression actually depend on PPARβ/δ or ERRα activation was not
466 studied. Here, through reporter gene assay, we have demonstrated that NCoR1 is a direct
467 corepressor of both PPARβ/δ and ERRα. Importantly, given that NCoR1 and PGC-1α
468 compete for the transcriptional regulation of PPARβ/δ and ERRα, our data indicate that
469 these transcription factors are common targets of both coregulators. Interestingly, we
470 observed a striking effect of the ERRα inverse agonist XCT790, since it completely inhibited
471 the increase in the mRNA level of several mitochondrial enzymes triggered by NCoR1
472 knockdown in cultured myotubes. These data are consistent with MARA results and suggest
473 that ERRα is the main target of NCoR1 in the control of muscle oxidative metabolism (Fig. 7).
474 Unexpectedly, we found that the PPARβ/δ selective antagonist GSK0660 did not affect the
475 effects of NCoR1 deletion on oxidative phosphorylation gene regulation. PPARβ/δ plays an
476 important role in the transcriptional control of lipid metabolism (13). Intriguingly, our
477 microarray analysis of NCoR1 MKO skeletal muscle shows a preferential enhancement of
478 oxidative phosphorylation and TCA cycle compared to the modulation of fatty acid β-
479 oxidation. Thus, it is conceivable that in our experimental context of animals fed with
480 normal chow, PPARβ/δ plays less of a role compared to studies using high fat diets (51) or
481 conditions like obesity and physical inactivity. NCoR1 might control fatty acid metabolism
482 through the transcriptional regulation of PPARβ/δ in an environment of elevated
483 intramyocellular lipids that could act as PPARβ/δ ligands, but this hypothesis needs to be
484 substantiated in future studies. Overall, it seems that a fully functional ERRα-PGC-

485 1α complex is a prerequisite for the improved oxidative metabolism induced by muscle-
486 specific NCoR1 deletion, at least in chow fed mice.
487 Interestingly, NCoR1 MKO mice have a milder oxidative phenotype compared to PGC-1α
488 transgenic mice. The weaker phenotype is also reflected in the quantitative differences in
489 gene expression. Thus, while the muscle knockout of NCoR1 resulted in the up-regulation of
490 21 genes involved in oxidative phosphorylation, 83 genes were increased in response to
491 muscle PGC-1α overexpression. Consistently, PGC-1α mTg mice exhibit a higher increase in
492 the VO_{2peak} (24%) (11) compared to NCoR1 MKO animals (7.2%). However, it is important to
493 note that NCoR1 is a basal corepressor, thus it represses transcription factors under basal
494 conditions and it is exchanged by coactivators upon a positive stimulus (17, 37). Therefore,
495 our data suggest that during basal conditions, NCoR1 deletion would not result in a full
496 activation of PPARβ/δ and ERRα, which subsequently could be amplified by a positive
497 stimulus such as exercise that is well known to increase PGC-1α expression (4) and thereby
498 unleashes the full activity of these transcription factors.
499 In conclusion, our data indicate competition between NCoR1 and PGC-1α in the regulation
500 of PPARβ/δ and ERRα transcriptional activity in skeletal muscle, of which the regulation of
501 ERRα represents the predominant regulatory mechanism of oxidative metabolism during
502 basal conditions (Fig. 7). The elucidation of different pharmacological or non-
503 pharmacological (e.g. exercise training) strategies to modulate NCoR1 activity and thus
504 facilitate PGC-1α action represents attractive strategies for the treatment of metabolic
505 diseases.
506

ACKNOWLEDGMENTS

We would like to thank Dr. Christopher K. Glass (University of California, San Diego), Dr. Junichi Sadoshima (University of Medicine and Dentistry of New Jersey) and Dr. Vincent Giguère (McGill University, Montreal) for their generous contribution with pFlag-NCoR, pERRE-luc and pERRα plasmids, respectively. We also thank Mr. Philippe Demougin (Biozentrum, University of Basel) for his help with microarray analysis and Dr. Hiroyasu Yamamoto for providing the LacZ and NCoR1 adenoviruses (Ecole Polytechnique Fédérale de Lausanne).

This project was funded by the Swiss National Science Foundation (SNF 310030_132900), the Muscular Dystrophy Association USA (MDA), the SwissLife 'Jubiläumsstiftung für Volksgesundheit und medizinische Forschung', the Swiss Society for Research on Muscle Diseases (SSEM), the Swiss Diabetes Association, the Roche Research Foundation, the United Mitochondrial Disease Foundation (UMDF), the Association Française contre les Myopathies (AFM), the Ecole Polytechnique Féderale de Lausanne, the European Research Council, and the University of Basel.

REFERENCES

1. **Al-Shahrour, F., R. Diaz-Uriarte, and J. Dopazo.** 2004. FatiGO: a web tool for finding significant associations of Gene Ontology terms with groups of genes. Bioinformatics **20:**578-580.

2. **Alenghat, T., K. Meyers, S. E. Mullican, K. Leitner, A. Adeniji-Adele, J. Avila, M. Bucan, R. S. Ahima, K. H. Kaestner, and M. A. Lazar.** 2008. Nuclear receptor corepressor and histone deacetylase 3 govern circadian metabolic physiology. Nature **456:**997-1000.

3. **Baar, K.** 2010. Epigenetic control of skeletal muscle fibre type. Acta Physiol (Oxf) **199:**477-487.

4. **Baar, K., A. R. Wende, T. E. Jones, M. Marison, L. A. Nolte, M. Chen, D. P. Kelly, and J. O. Holloszy.** 2002. Adaptations of skeletal muscle to exercise: rapid increase in the transcriptional coactivator PGC-1. Faseb J **16:**1879-1886.

5. **Bailey, P., M. Downes, P. Lau, J. Harris, S. L. Chen, Y. Hamamori, V. Sartorelli, and G. E. Muscat.** 1999. The nuclear receptor corepressor N-CoR regulates differentiation: N-CoR directly interacts with MyoD. Mol Endocrinol **13:**1155-1168.

6. **Barres, R., J. Yan, B. Egan, J. T. Treebak, M. Rasmussen, T. Fritz, K. Caidahl, A. Krook, D. J. O'Gorman, and J. R. Zierath.** 2012. Acute exercise remodels promoter methylation in human skeletal muscle. Cell Metab **15:**405-411.

7. **Bassel-Duby, R., and E. N. Olson.** 2006. Signaling pathways in skeletal muscle remodeling. Annu Rev Biochem **75:**19-37.

8. **Booth, F. W., and S. J. Lees.** 2007. Fundamental questions about genes, inactivity, and chronic diseases. Physiol Genomics **28:**146-157.

9. **Booth, F. W., and C. K. Roberts.** 2008. Linking performance and chronic disease risk: indices of physical performance are surrogates for health. Br J Sports Med **42:**950-952.

10. **Busson, M., A. Carazo, P. Seyer, S. Grandemange, F. Casas, L. Pessemesse, J. P. Rouault, C. Wrutniak-Cabello, and G. Cabello.** 2005. Coactivation of nuclear receptors and myogenic factors induces the major BTG1 influence on muscle differentiation. Oncogene **24:**1698-1710.

11. **Calvo, J. A., T. G. Daniels, X. Wang, A. Paul, J. Lin, B. M. Spiegelman, S. C. Stevenson, and S. M. Rangwala.** 2008. Muscle-specific expression of PPARgamma coactivator-1alpha improves exercise performance and increases peak oxygen uptake. J Appl Physiol **104:**1304-1312.

12. **Charest-Marcotte, A., C. R. Dufour, B. J. Wilson, A. M. Tremblay, L. J. Eichner, D. H. Arlow, V. K. Mootha, and V. Giguere.** 2010. The homeobox protein Prox1 is a negative modulator of ERR{alpha}/PGC-1{alpha} bioenergetic functions. Genes Dev **24:**537-542.

13. **Ehrenborg, E., and A. Krook.** 2009. Regulation of skeletal muscle physiology and metabolism by peroxisome proliferator-activated receptor delta. Pharmacol Rev **61:**373-393.

14. **Fischle, W., F. Dequiedt, M. J. Hendzel, M. G. Guenther, M. A. Lazar, W. Voelter, and E. Verdin.** 2002. Enzymatic activity associated with class II HDACs is dependent on a multiprotein complex containing HDAC3 and SMRT/N-CoR. Mol Cell **9:**45-57.

15. **Furuya, F., C. J. Guigon, L. Zhao, C. Lu, J. A. Hanover, and S. Y. Cheng.** 2007. Nuclear receptor corepressor is a novel regulator of phosphatidylinositol 3-kinase signaling. Mol Cell Biol **27:**6116-6126.

16. **Giguere, V.** 2008. Transcriptional control of energy homeostasis by the estrogen-related receptors. Endocr Rev **29:**677-696.

17. **Glass, C. K., and M. G. Rosenfeld.** 2000. The coregulator exchange in transcriptional functions of nuclear receptors. Genes Dev **14:**121-141.

18. **Gonzalez, E., and O. Delbono.** 2001. Age-dependent fatigue in single intact fast- and slow fibers from mouse EDL and soleus skeletal muscles. Mech Ageing Dev **122:**1019-1032.

19. **Handschin, C., and B. M. Spiegelman.** 2008. The role of exercise and PGC1alpha in inflammation and chronic disease. Nature **454:**463-469.

20. **Hardie, D. G., F. A. Ross, and S. A. Hawley.** 2012. AMPK: a nutrient and energy sensor that maintains energy homeostasis. Nat Rev Mol Cell Biol **13:**251-262.

21. **Hawley, S. A., M. D. Fullerton, F. A. Ross, J. D. Schertzer, C. Chevtzoff, K. J. Walker, M. W. Peggie, D. Zibrova, K. A. Green, K. J. Mustard, B. E. Kemp, K. Sakamoto, G. R. Steinberg, and D. G. Hardie.** 2012. The ancient drug salicylate directly activates AMP-activated protein kinase. Science **336:**918-922.

22. **Horlein, A. J., A. M. Naar, T. Heinzel, J. Torchia, B. Gloss, R. Kurokawa, A. Ryan, Y. Kamei, M. Soderstrom, C. K. Glass, and et al.** 1995. Ligand-independent repression by the thyroid hormone receptor mediated by a nuclear receptor co-repressor. Nature **377:**397-404.

23. **Ishizuka, T., and M. A. Lazar.** 2005. The nuclear receptor corepressor deacetylase activating domain is essential for repression by thyroid hormone receptor. Mol Endocrinol **19:**1443-1451.

24. **Jepsen, K., O. Hermanson, T. M. Onami, A. S. Gleiberman, V. Lunyak, R. J. McEvilly, R. Kurokawa, V. Kumar, F. Liu, E. Seto, S. M. Hedrick, G. Mandel, C. K. Glass, D. W. Rose, and M. G. Rosenfeld.** 2000. Combinatorial roles of the nuclear receptor corepressor in transcription and development. Cell **102:**753-763.

25. **Kelley, D. E., J. He, E. V. Menshikova, and V. B. Ritov.** 2002. Dysfunction of mitochondria in human skeletal muscle in type 2 diabetes. Diabetes **51:**2944-2950.

26. **Kitamura, T., Y. I. Kitamura, Y. Funahashi, C. J. Shawber, D. H. Castrillon, R. Kollipara, R. A. DePinho, J. Kitajewski, and D. Accili.** 2007. A Foxo/Notch pathway controls myogenic differentiation and fiber type specification. J Clin Invest **117:**2477-2485.

27. **Kouzarides, T.** 2007. Chromatin modifications and their function. Cell **128:**693-705.

28. **Li, P., W. Fan, J. Xu, M. Lu, H. Yamamoto, J. Auwerx, D. D. Sears, S. Talukdar, D. Oh, A. Chen, G. Bandyopadhyay, M. Scadeng, J. M. Ofrecio, S. Nalbandian, and J. M. Olefsky.** 2011. Adipocyte NCoR Knockout Decreases PPARgamma Phosphorylation and Enhances PPARgamma Activity and Insulin Sensitivity. Cell **147:**815-826.

29. **Lin, J., C. Handschin, and B. M. Spiegelman.** 2005. Metabolic control through the PGC-1 family of transcription coactivators. Cell Metab **1:**361-370.

30. **Lin, J., H. Wu, P. T. Tarr, C. Y. Zhang, Z. Wu, O. Boss, L. F. Michael, P. Puigserver, E. Isotani, E. N. Olson, B. B. Lowell, R. Bassel-Duby, and B. M. Spiegelman.** 2002. Transcriptional co-activator PGC-1 alpha drives the formation of slow-twitch muscle fibres. Nature **418:**797-801.

31. **McGee, S. L., and M. Hargreaves.** 2011. Histone modifications and exercise adaptations. J Appl Physiol **110:**258-263.

32. **McKenna, N. J., and B. W. O'Malley.** 2010. SnapShot: NR coregulators. Cell **143:**172-172 e171.

33. **Mootha, V. K., C. Handschin, D. Arlow, X. Xie, J. St Pierre, S. Sihag, W. Yang, D. Altshuler, P. Puigserver, N. Patterson, P. J. Willy, I. G. Schulman, R. A. Heyman, E. S. Lander, and B. M. Spiegelman.** 2004. Erralpha and Gabpa/b specify PGC-1alpha-dependent oxidative phosphorylation gene expression that is altered in diabetic muscle. Proc Natl Acad Sci U S A **101:**6570-6575.

34. **Mootha, V. K., C. M. Lindgren, K. F. Eriksson, A. Subramanian, S. Sihag, J. Lehar, P. Puigserver, E. Carlsson, M. Ridderstrale, E. Laurila, N. Houstis, M. J. Daly, N. Patterson, J. P. Mesirov, T. R. Golub, P. Tamayo, B. Spiegelman, E. S. Lander, J. N. Hirschhorn, D. Altshuler, and L. C. Groop.** 2003. PGC-1alpha-responsive genes involved in oxidative phosphorylation are coordinately downregulated in human diabetes. Nat Genet **34:**267-273.

35. **Nuutila, P., M. J. Knuuti, O. J. Heinonen, U. Ruotsalainen, M. Teras, J. Bergman, O. Solin, H. Yki-Jarvinen, L. M. Voipio-Pulkki, U. Wegelius, and et al.** 1994. Different alterations in the insulin-stimulated glucose uptake in the athlete's heart and skeletal muscle. J Clin Invest **93:**2267-2274.

36. **Oka, S., R. Alcendor, P. Zhai, J. Y. Park, D. Shao, J. Cho, T. Yamamoto, B. Tian, and J. Sadoshima.** 2011. PPARalpha-Sirt1 complex mediates cardiac hypertrophy and failure through suppression of the ERR transcriptional pathway. Cell Metab **14:**598-611.

37. **Perissi, V., A. Aggarwal, C. K. Glass, D. W. Rose, and M. G. Rosenfeld.** 2004. A corepressor/coactivator exchange complex required for transcriptional activation by nuclear receptors and other regulated transcription factors. Cell **116:**511-526.

38. **Petersen, K. F., S. Dufour, D. Befroy, R. Garcia, and G. I. Shulman.** 2004. Impaired mitochondrial activity in the insulin-resistant offspring of patients with type 2 diabetes. N Engl J Med **350:**664-671.

39. **Potthoff, M. J., H. Wu, M. A. Arnold, J. M. Shelton, J. Backs, J. McAnally, J. A. Richardson, R. Bassel-Duby, and E. N. Olson.** 2007. Histone deacetylase degradation and MEF2 activation promote the formation of slow-twitch myofibers. J Clin Invest **117:**2459-2467.

40. **Reilly, S. M., P. Bhargava, S. Liu, M. R. Gangl, C. Gorgun, R. R. Nofsinger, R. M. Evans, L. Qi, F. B. Hu, and C. H. Lee.** 2010. Nuclear receptor corepressor SMRT regulates mitochondrial oxidative metabolism and mediates aging-related metabolic deterioration. Cell Metab **12:**643-653.

41. **Santos, G. M., L. Fairall, and J. W. Schwabe.** 2011. Negative regulation by nuclear receptors: a plethora of mechanisms. Trends Endocrinol Metab **22:**87-93.

42. **Schuler, M. J., S. Buhler, and D. Pette.** 1999. Effects of contractile activity and hypothyroidism on nuclear hormone receptor mRNA isoforms in rat skeletal muscle. Eur J Biochem **264:**982-988.

43. **Schuler, M. J., and D. Pette.** 1998. Quantification of thyroid hormone receptor isoforms, 9-cis retinoic acid receptor gamma, and nuclear receptor co-repressor by reverse-transcriptase PCR in maturing and adult skeletal muscles of rat. Eur J Biochem **257:**607-614.

44. **Shearer, B. G., D. J. Steger, J. M. Way, T. B. Stanley, D. C. Lobe, D. A. Grillot, M. A. Iannone, M. A. Lazar, T. M. Willson, and A. N. Billin.** 2008. Identification and characterization of a selective peroxisome proliferator-activated receptor beta/delta (NR1C2) antagonist. Mol Endocrinol **22:**523-529.

45. **Summermatter, S., R. Thurnheer, G. Santos, B. Mosca, O. Baum, S. Treves, H. Hoppeler, F. Zorzato, and C. Handschin.** 2012. Remodeling of calcium handling in

skeletal muscle through PGC-1alpha: impact on force, fatigability, and fiber type. Am J Physiol Cell Physiol **302:**C88-99.

46. **Sutanto, M. M., K. K. Ferguson, H. Sakuma, H. Ye, M. J. Brady, and R. N. Cohen.** 2010. The silencing mediator of retinoid and thyroid hormone receptors (SMRT) regulates adipose tissue accumulation and adipocyte insulin sensitivity in vivo. J Biol Chem **285:**18485-18495.

47. **Suzuki, H., A. R. Forrest, E. van Nimwegen, C. O. Daub, P. J. Balwierz, K. M. Irvine, T. Lassmann, T. Ravasi, Y. Hasegawa, M. J. de Hoon, S. Katayama, K. Schroder, P. Carninci, Y. Tomaru, M. Kanamori-Katayama, A. Kubosaki, A. Akalin, Y. Ando, E. Arner, M. Asada, H. Asahara, T. Bailey, V. B. Bajic, D. Bauer, A. G. Beckhouse, N. Bertin, J. Bjorkegren, F. Brombacher, E. Bulger, A. M. Chalk, J. Chiba, N. Cloonan, A. Dawe, J. Dostie, P. G. Engstrom, M. Essack, G. J. Faulkner, J. L. Fink, D. Fredman, K. Fujimori, M. Furuno, T. Gojobori, J. Gough, S. M. Grimmond, M. Gustafsson, M. Hashimoto, T. Hashimoto, M. Hatakeyama, S. Heinzel, W. Hide, O. Hofmann, M. Hornquist, L. Huminiecki, K. Ikeo, N. Imamoto, S. Inoue, Y. Inoue, R. Ishihara, T. Iwayanagi, A. Jacobsen, M. Kaur, H. Kawaji, M. C. Kerr, R. Kimura, S. Kimura, Y. Kimura, H. Kitano, H. Koga, T. Kojima, S. Kondo, T. Konno, A. Krogh, A. Kruger, A. Kumar, B. Lenhard, A. Lennartsson, M. Lindow, M. Lizio, C. Macpherson, N. Maeda, C. A. Maher, M. Maqungo, J. Mar, N. A. Matigian, H. Matsuda, J. S. Mattick, S. Meier, S. Miyamoto, E. Miyamoto-Sato, K. Nakabayashi, Y. Nakachi, M. Nakano, S. Nygaard, T. Okayama, Y. Okazaki, H. Okuda-Yabukami, V. Orlando, J. Otomo, M. Pachkov, N. Petrovsky, et al.** 2009. The transcriptional network that controls growth arrest and differentiation in a human myeloid leukemia cell line. Nat Genet **41:**553-562.

48. **Webb, P., C. M. Anderson, C. Valentine, P. Nguyen, A. Marimuthu, B. L. West, J. D. Baxter, and P. J. Kushner.** 2000. The nuclear receptor corepressor (N-CoR) contains three isoleucine motifs (I/LXXII) that serve as receptor interaction domains (IDs). Mol Endocrinol **14:**1976-1985.

49. **Willy, P. J., I. R. Murray, J. Qian, B. B. Busch, W. C. Stevens, Jr., R. Martin, R. Mohan, S. Zhou, P. Ordentlich, P. Wei, D. W. Sapp, R. A. Horlick, R. A. Heyman, and I. G. Schulman.** 2004. Regulation of PPARgamma coactivator 1alpha (PGC-1alpha) signaling by an estrogen-related receptor alpha (ERRalpha) ligand. Proc Natl Acad Sci U S A **101:**8912-8917.

50. **Wisloff, U., S. M. Najjar, O. Ellingsen, P. M. Haram, S. Swoap, Q. Al-Share, M. Fernstrom, K. Rezaei, S. J. Lee, L. G. Koch, and S. L. Britton.** 2005. Cardiovascular risk factors emerge after artificial selection for low aerobic capacity. Science **307:**418-420.

51. **Yamamoto, H., E. G. Williams, L. Mouchiroud, C. Canto, W. Fan, M. Downes, C. Heligon, G. D. Barish, B. Desvergne, R. M. Evans, K. Schoonjans, and J. Auwerx.** 2011. NCoR1 Is a Conserved Physiological Modulator of Muscle Mass and Oxidative Function. Cell **147:**827-839.

52. **Yoon, H. G., D. W. Chan, Z. Q. Huang, J. Li, J. D. Fondell, J. Qin, and J. Wong.** 2003. Purification and functional characterization of the human N-CoR complex: the roles of HDAC3, TBL1 and TBLR1. Embo J **22:**1336-1346.

FIGURE LEGENDS

FIG 1 Exercise performance and in vivo contractile properties of NCoR1 MKO mice skeletal muscle. (A) VO_2 during the maximal exercise test (n = 8 CON and n = 7 NCoR1 MKO). (B and C) Representative pictures and quantification of NADH (B) and PAS (C) staining of tibialis anterior (n = 3-4 CON and n = 3-4 NCoR1 MKO). (D) Representative blots and quantification of gastrocnemius AMPK phosphorylation levels (n = 7 CON and n = 4 NCoR1 MKO). (E and F) In vivo assessment of maximal grip strength and isometric muscle fatigue resistance (n = 13 CON and n = 12 NCoR1 MKO). Values represent mean ± SEM. *p < 0.05, **p < 0.01, ***p < 0.001 CON vs. NCoR1 MKO.

FIG 2 Ex vivo contractile properties of NCoR1 MKO mice skeletal muscle. (A-D) Ex vivo assessment of extensor digitorum longus (EDL) and soleus (SOL) contractility in response to a single twitch or a maximal tetanic stimulation (n = 10 CON and n = 14 NCoR1 MKO muscles per group). (E and F) Ex vivo assessment of EDL and SOL fatigue resistance in response to repeated tetanic stimulation through a long and short interval protocol. Inset (F) shows the section with significant differences (n = 10 CON and n = 14 MKO muscles per group). Values represent mean ± SEM. *p < 0.05, **p < 0.01 CON vs. MKO.

FIG 3 Similarities between NCoR1 MKO and PGC-1α mTg mice on oxidative metabolism. (A and B) Top 5 KEGG pathways from GO analysis of the up- and down-regulated genes from the NCoR1 MKO and PGC-1α mTg microarray data sets (n = 5 per group). (C) Venn diagrams showing the overlap between NCoR1 MKO and PGC-1α mTG microarray data sets. (D and E) Heat maps generated using probe-set intensities of the overlapping transcripts between NCoR1 MKO and PGC-1α mTg related to the GO terms “oxidative phosphorylation (OXHPOS)” and “citrate cycle (TCA cycle)”. (F) Real-Time PCR analysis of mRNA levels of

mitochondrial encoded genes of gastrocnemius from CON (n = 7) and NCoR1 MKO (n = 5) animals. (G) Measurement of mitochondrial DNA (mtDNA) content of gastrocnemius from CON (n = 7) and NCoR1 MKO (n = 5) animals. Values represent mean ± SEM. *p < 0.05, **p < 0.01 CON vs. NCoR1 MKO.

FIG 4 Role of PGC-1α/β in NCoR1 regulation of oxidative metabolism. (A) Gastrocnemius (GAS) mRNA levels of PGC-1 family of coactivators (n = 7 CON and n = 5 NCoR1 MKO). (B to D) Adenoviral knockdown (KD) of LacZ (CON) or NCoR1 alone or in combination with PGC-1α or PGC-1β KD for 48 h in C_2C_{12} myotubes (n = 3 independent experiments performed in triplicate each). Values represent mean ± SEM. *p < 0.05, **p < 0.01, ***p < 0.001 CON vs. MKO or as indicated.

FIG 5 Identification of common transcription factor binding partners of NCoR1 and PGC-1α. (A and B) The top 4 transcription factors motifs exhibiting increased and decreased activity in MARA of the microarray data performed on gastrocnemius from NCoR1 MKO and PGC-1α mTg mice (n = 5 per group). (C-F) Changes in the activity of RXRs and ERRα (ESRRA) in NCoR1 MKO and PGC-1α mTg skeletal muscle predicted by MARA analysis of microarray data (n = 5 per group). (G) Venn diagrams showing the overlap between NCoR1 MKO and PGC-1α mTg MARA analysis.

FIG 6 Role of PPARβ/δ and ERRα in NCoR1 regulation of oxidative metabolism. (A) Gastrocnemius mRNA levels of different transcriptions factors (n = 7 CON and n = 5 NCoR1 MKO). RXR: retinoid X receptor, PPAR: peroxisome proliferator activated receptor, ERR: estrogen-related receptor and TFAM: transcription factor A, mitochondrial. (B and C) Luciferase activity of PPRE-luc and ERRE-luc reporter plasmids in COS-7 cells co-transfected with PPARβ/δ, ERRα, NCoR1 and PGC-1α as indicated in each figure (n = 5 independent

experiments performed in triplicate each). (D and E) Adenoviral knockdown (KD) of LacZ (CON) or NCoR1 alone or in combination with 10 μM XCT790 or 1 μM GSK0660 for 48 h in C_2C_{12} myotubes (n = 3 independent experiments performed in triplicate each). Values represent mean ± SEM. *p < 0.05, **p < 0.01, ***p < 0.001 CON vs. NCoR1 MKO or as indicated.

FIG 7 Antagonistic regulation of oxidative metabolism by NCoR1 and PGC-1α. Proposed mechanism by which NCoR1 and PGC-1α complexes compete for the transcriptional regulation of ERRα and, as a consequence, oxidative metabolism. Under basal and possibly pathological conditions, NCoR1 represses ERRα and increases histone deacetylation, thereby decreasing metabolic gene transcription. In contrast, PGC-1α is activated by exercise and caloric restriction in skeletal muscle, coactivates ERRα and consequently enhances mitochondrial function. ERRE: ERR response elements, Ac: histone acetylation.

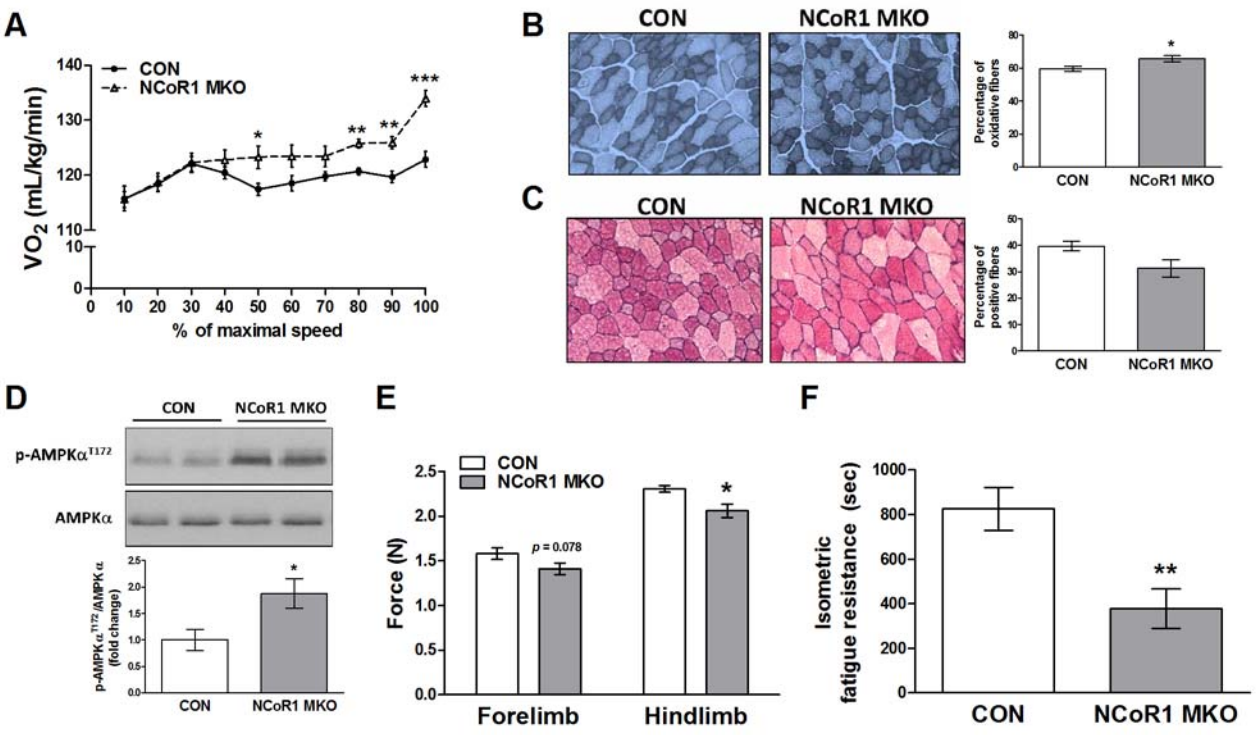
A
CON
NCoR1 MKO
VO2 (mL/kg/min)
% of maximal speed
B
CON
NCoR1 MKO
Percentage of oxidative fibers
C
CON
NCoR1 MKO
Percentage of positive fibers
D
CON
NCoR1 MKO
p-AMPKα T172
AMPKα
p-AMPKα T172/AMPK α (fold change)
E
CON
NCoR1 MKO
p = 0.078
Force (N)
Forelimb
Hindlimb
F
Isometric fatigue resistance (sec)
CON
NCoR1 MKO

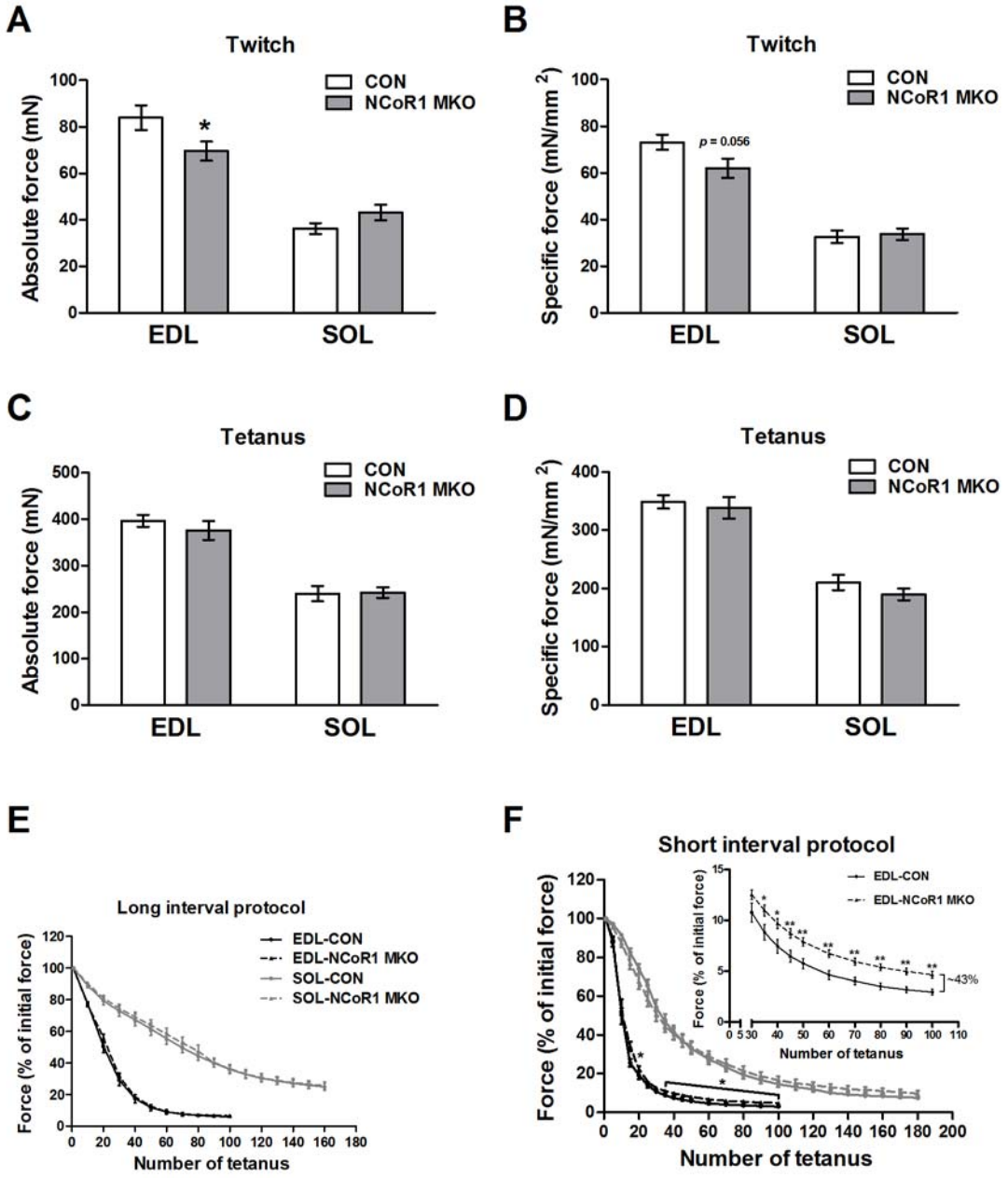
A
Twitch
CON
NCoR1 MKO
Absolute force (mN)
EDL
SOL
B
Twitch
CON
NCoR1 MKO
p = 0.056
Specific force (mN/mm 2)
EDL
SOL
C
Tetanus
CON
NCoR1 MKO
Absolute force (mN)
EDL
SOL
D
Tetanus
CON
NCoR1 MKO
Specific force (mN/mm 2)
EDL
SOL
E
Long interval protocol
EDL-CON
EDL-NCoR1 MKO
SOL-CON
SOL-NCoR1 MKO
Force (% of initial force)
Number of tetanus
F
Short interval protocol
EDL-CON
EDL-NCoR1 MKO
~43%
Force (% of initial force)
Number of tetanus

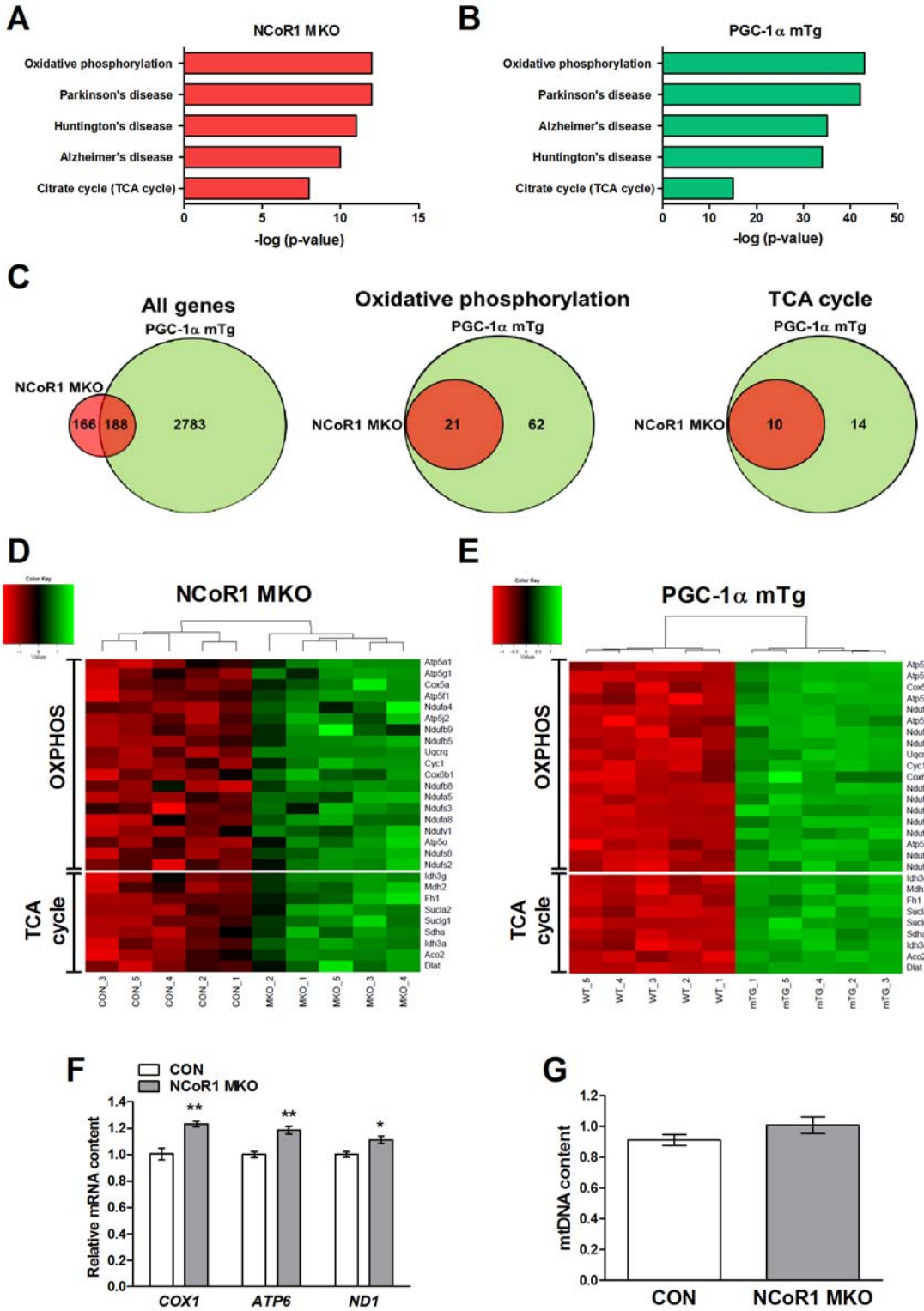
A
NCoR1 MKO
Oxidative phosphorylation
Parkinson's disease
Huntington's disease
Alzheimer's disease
Citrate cycle (TCA cycle)
0
5
10
15
-log (p-value)
B
PGC-1α mTg
Oxidative phosphorylation
Parkinson's disease
Alzheimer's disease
Huntington's disease
Citrate cycle (TCA cycle)
0
10
20
30
40
50
-log (p-value)
C
All genes
PGC-1α mTg
NCoR1 MKO
166
188
2783
Oxidative phosphorylation
PGC-1α mTg
NCoR1 MKO
21
62
TCA cycle
PGC-1α mTg
NCoR1 MKO
10
14
D
NCoR1 MKO
OXPHOS
TCA cycle
Atp5a1
Atp5g1
Cox5a
Atp5f1
Ndufa4
Atp5j2
Ndufb9
Ndufb5
Uqcrq
Cyc1
Cox6b1
Ndufb8
Ndufa5
Ndufs3
Ndufa8
Ndufv1
Atp5o
Ndufs8
Ndufs2
Idh3g
Mdh2
Fh1
Sucla2
Suclg1
Sdha
Idh3a
Aco2
Dlat
CON_3
CON_5
CON_4
CON_2
CON_1
MKO_2
MKO_1
MKO_5
MKO_3
MKO_4
E
PGC-1α mTg
OXPHOS
TCA cycle
WT_5
WT_4
WT_3
WT_2
WT_1
mTG_1
mTG_5
mTG_4
mTG_2
mTG_3
F
CON
NCoR1 MKO
Relative mRNA content
0.0
0.2
0.4
0.6
0.8
1.0
1.2
1.4
**
**
*
COX1
ATP6
ND1
G
mtDNA content
0.0
0.2
0.4
0.6
0.8
1.0
1.2
CON
NCoR1 MKO

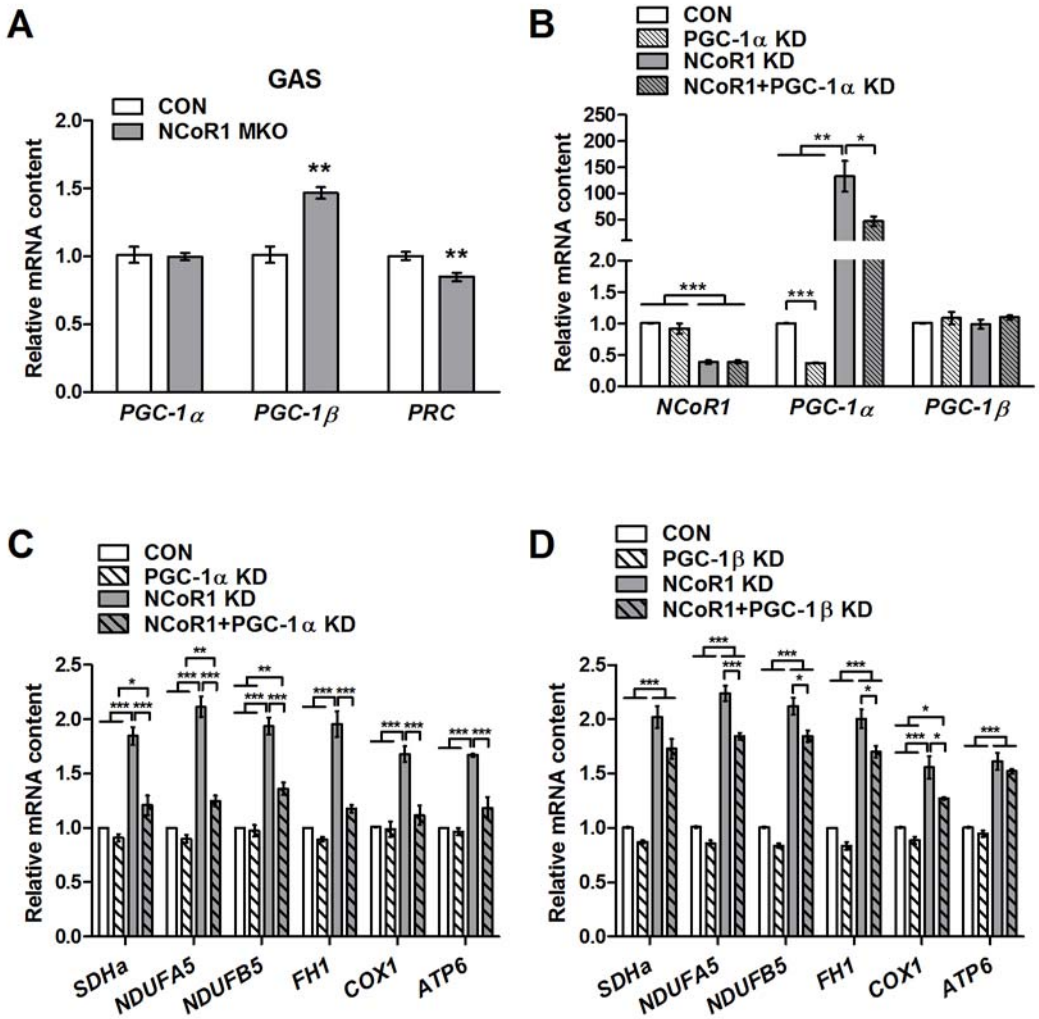
A
GAS
CON
NCoR1 MKO
Relative mRNA content
PGC-1α
PGC-1β
PRC
B
CON
PGC-1α KD
NCoR1 KD
NCoR1+PGC-1α KD
Relative mRNA content
NCoR1
PGC-1α
PGC-1β
C
CON
PGC-1α KD
NCoR1 KD
NCoR1+PGC-1α KD
Relative mRNA content
SDHa
NDUFA5
NDUFB5
FH1
COX1
ATP6
D
CON
PGC-1β KD
NCoR1 KD
NCoR1+PGC-1β KD
Relative mRNA content
SDHa
NDUFA5
NDUFB5
FH1
COX1
ATP6

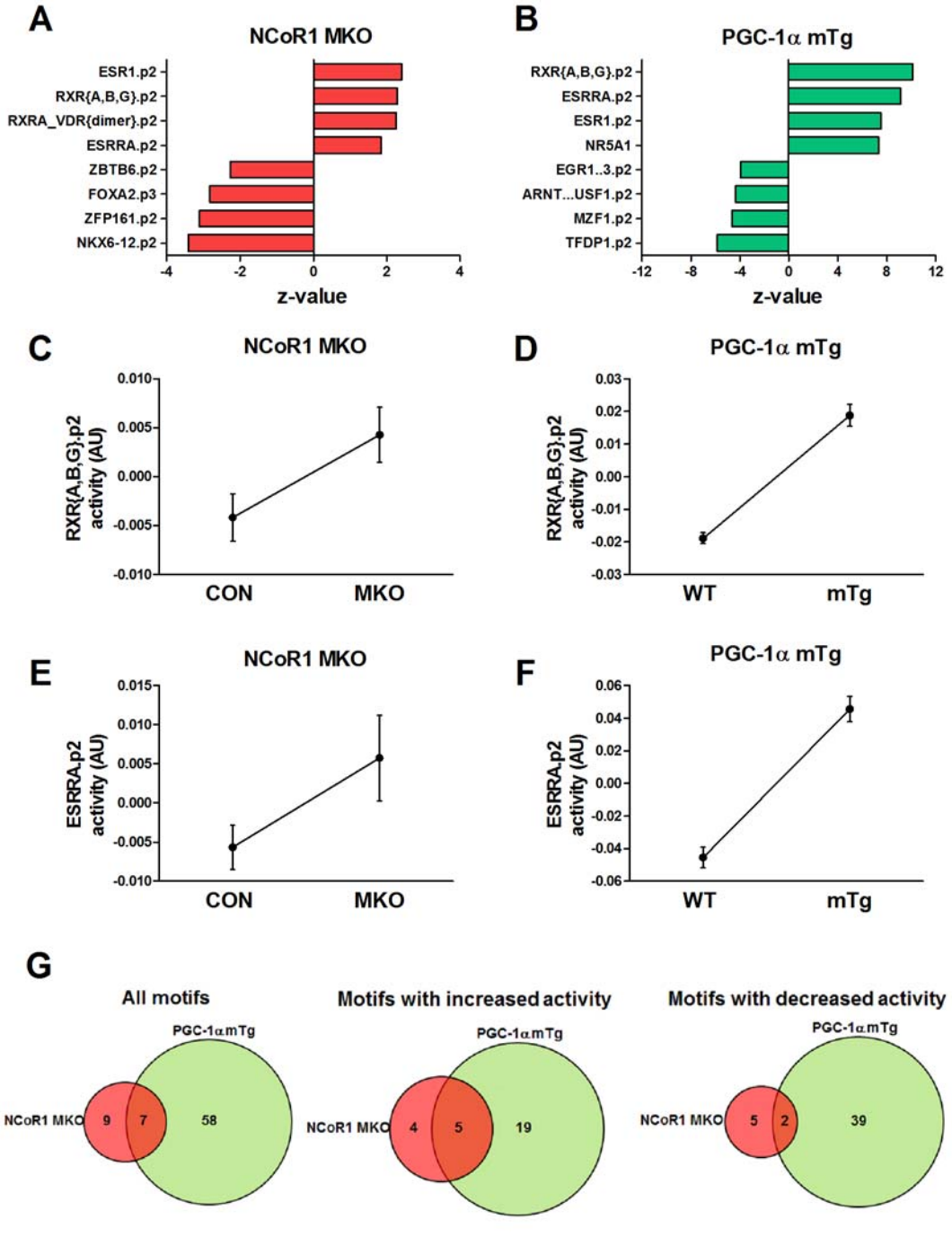
A
NCoR1 MKO
ESR1.p2
RXR{A,B,G}.p2
RXRA_VDR{dimer}.p2
ESRRA.p2
ZBTB6.p2
FOXA2.p3
ZFP161.p2
NKX6-12.p2
-4
-2
0
2
4
z-value
B
PGC-1α mTg
RXR{A,B,G}.p2
ESRRA.p2
ESR1.p2
NR5A1
EGR1..3.p2
ARNT...USF1.p2
MZF1.p2
TFDP1.p2
-12
-8
-4
0
4
8
12
z-value
C
NCoR1 MKO
RXR{A,B,G}.p2 activity (AU)
0.010
0.005
0.000
-0.005
-0.010
CON
MKO
D
PGC-1α mTg
RXR{A,B,G}.p2 activity (AU)
0.03
0.02
0.01
0.00
-0.01
-0.02
-0.03
WT
mTg
E
NCoR1 MKO
ESRRA.p2 activity (AU)
0.015
0.010
0.005
0.000
-0.005
-0.010
CON
MKO
F
PGC-1α mTg
ESRRA.p2 activity (AU)
0.06
0.04
0.02
0.00
-0.02
-0.04
-0.06
WT
mTg
G
All motifs
PGC-1αmTg
NCoR1 MKO
9
7
58
Motifs with increased activity
PGC-1αmTg
NCoR1 MKO
4
5
19
Motifs with decreased activity
PGC-1αmTg
NCoR1 MKO
5
2
39

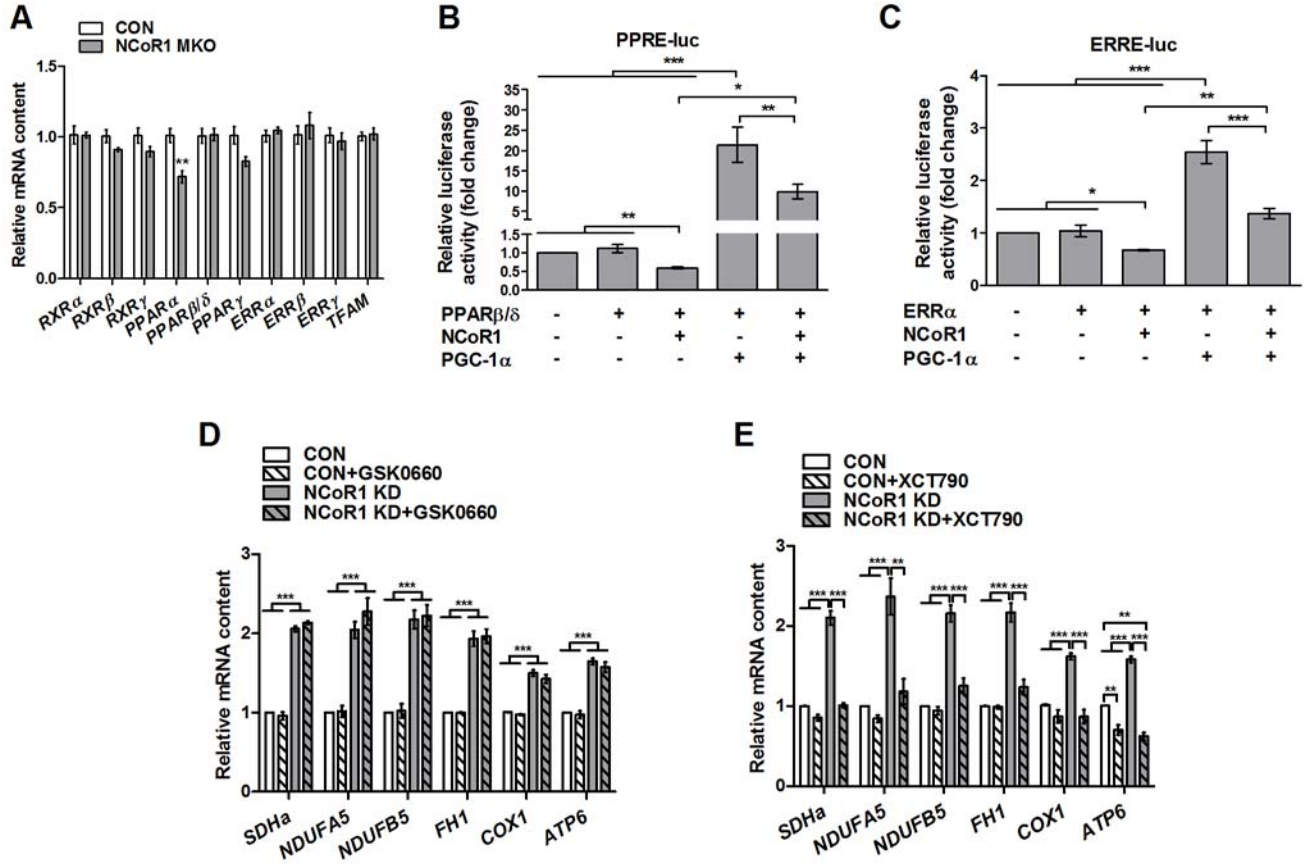
A
CON
NCoR1 MKO
Relative mRNA content
RXRα
RXRβ
RXRγ
PPARα
PPARβ/δ
PPARγ
ERRα
ERRβ
ERRγ
TFAM
B
PPRE-luc
Relative luciferase activity (fold change)
PPARβ/δ
NCoR1
PGC-1α
C
ERRE-luc
Relative luciferase activity (fold change)
ERRα
NCoR1
PGC-1α
D
CON
CON+GSK0660
NCoR1 KD
NCoR1 KD+GSK0660
Relative mRNA content
SDHa
NDUFA5
NDUFB5
FH1
COX1
ATP6
E
CON
CON+XCT790
NCoR1 KD
NCoR1 KD+XCT790
Relative mRNA content
SDHa
NDUFA5
NDUFB5
FH1
COX1
ATP6

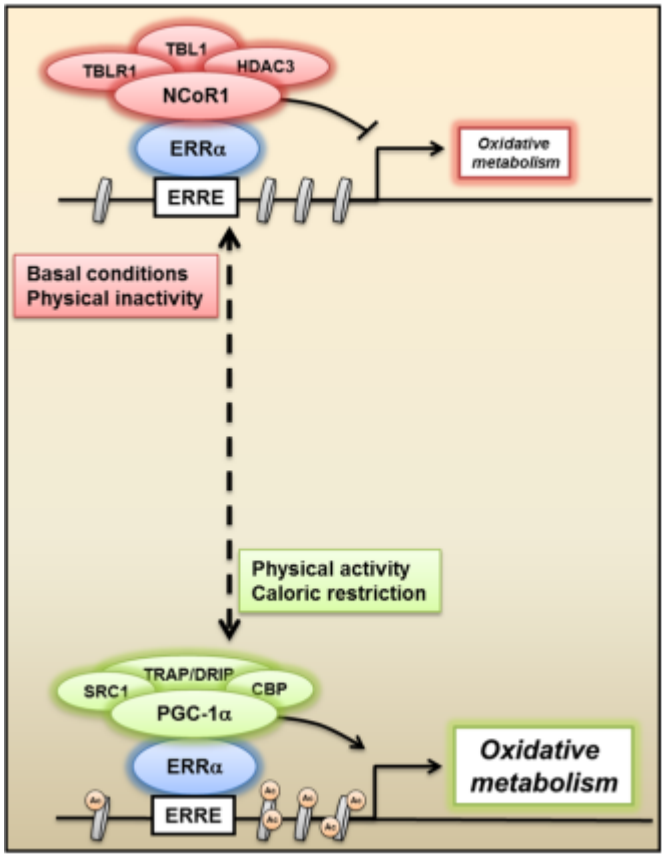
TBL1
TBLR1
HDAC3
NCoR1
ERRα
ERRE
Oxidative metabolism
Basal conditions
Physical inactivity
Physical activity
Caloric restriction
TRAP/DRIP
SRC1
CBP
PGC-1α
ERRα
ERRE
Oxidative metabolism

SUPPLEMENTAL MATERIAL

Fig. S1

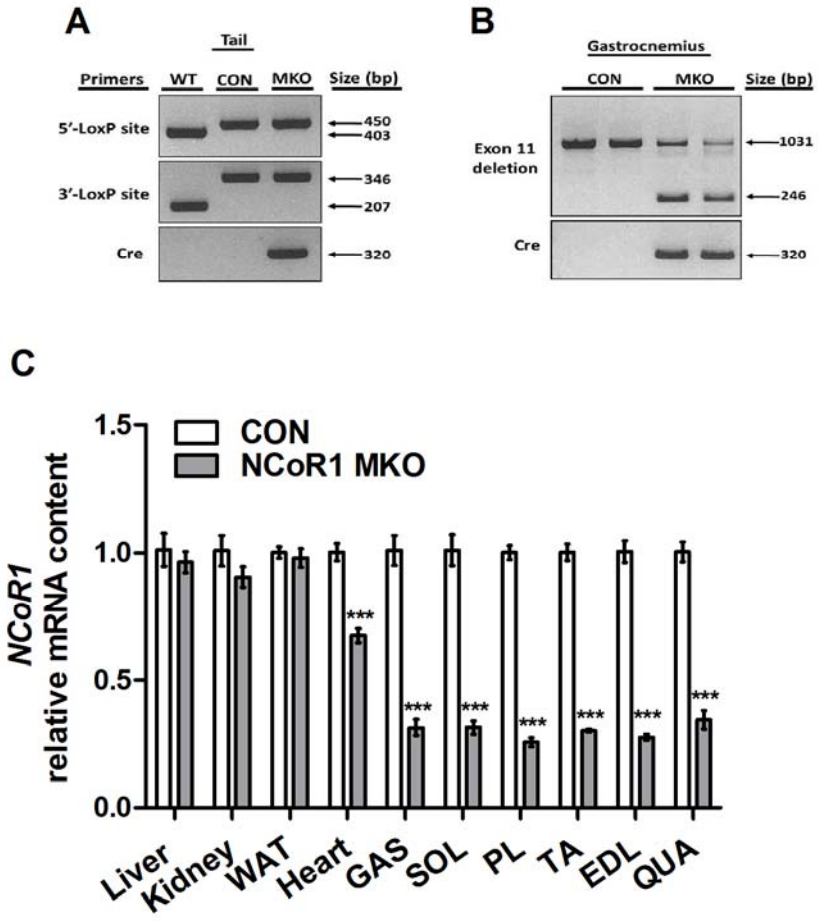

FIG S1 Specific deletion of NCoR1 in striated muscle. (*A* and *B*) PCR genotyping of wild type (WT), CON and NCoR1 MKO mice. (*A*) LoxP sites flanking exon 11 of *Ncor1* gene and the presence of *Cre* were detected from genomic DNA from the tail. (*B*) Recombination was assessed from genomic DNA from gastrocnemius. (*C*) NCoR1 mRNA levels in liver, kidney, white adipose tissue (WAT), heart, gastrocnemius (GAS), soleus (SOL), plantaris (PL), tibialis anterior (TA), extensor digitorum longus (EDL) and quadriceps (QUA) of CON (n = 7) and

NCoR1 MKO (n = 5) animals. Values represent mean ± SEM. ***$p < 0.001$ CON vs. NCoR1 MKO.

Fig. S2

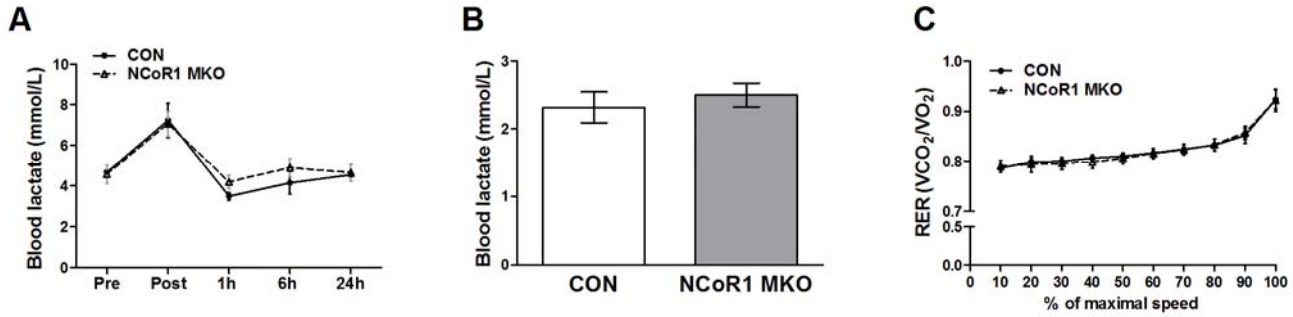

FIG S2 Indirect calorimetry during maximal exercise and blood lactate measurement. (A and B) Blood lactate determination before and after exercise (A), or in fasted (B) animals (n = 6 CON and n = 7 NCoR1 MKO). (C) Respiratory exchange ratio (RER) during the maximal exercise test (n = 8 CON and n = 7 NCoR1 MKO).. Values represent mean ± SEM.

Fig. S3

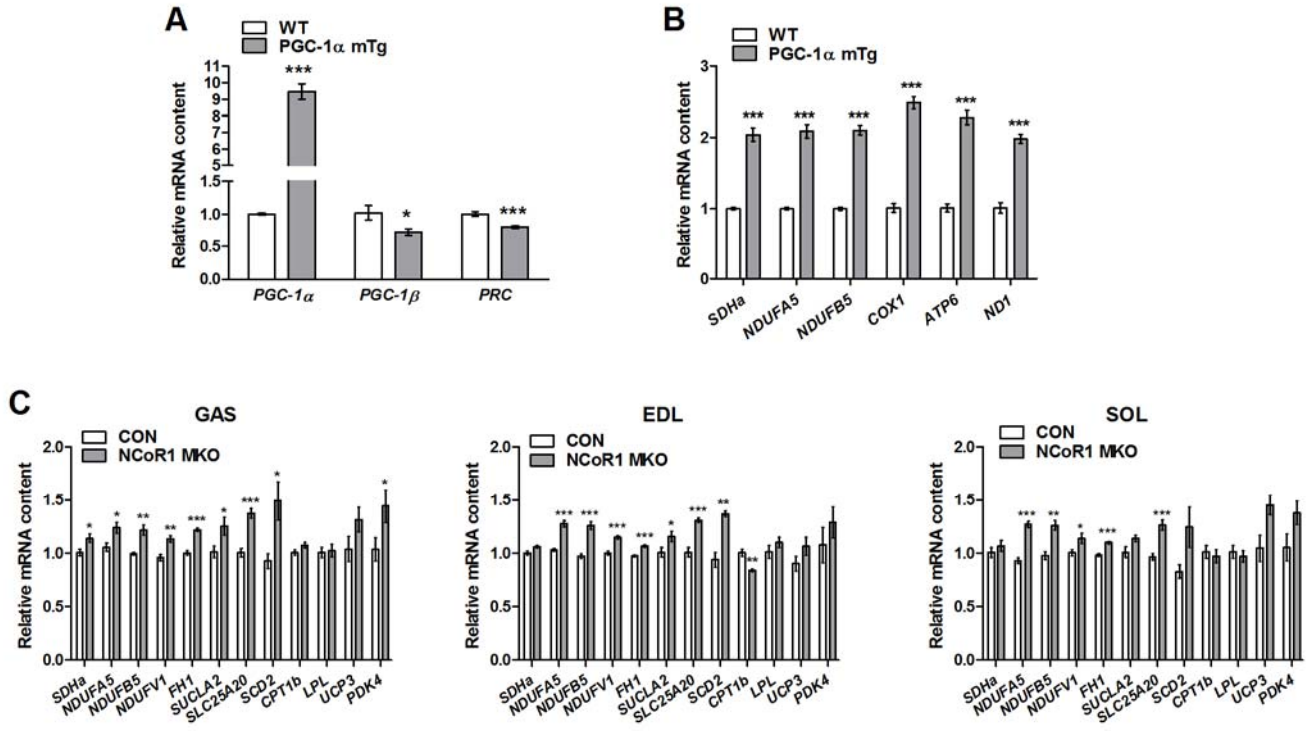

FIG S 3 PGC-1 levels in PGC-1α mTg mice and validation of microarray analysis. (*A*) mRNA level of PGC-1α, PGC-1β and PRC in gastrocnemius from wild type (WT) and PGC-1α mTg animals (n = 5 WT and n = 5 PGC-1α mTg). (*B*) Real-Time PCR analysis of several up-regulated genes from the microarray and mitochondrial encoded genes in WT and PGC-1α mTg gastrocnemius (n = 5 WT and n = 5 PGC-1α mTg). (*C*) Real-Time PCR analysis of several up-regulated genes from the microarray and different PPARβ/δ target genes in gastrocnemius (GAS), extensor digitorum longus (EDL) and soleus (SOL) (n = 7 CON and n = 5 NCoR1 MKO). Values represent mean ± SEM. *$p < 0.05$, **$p < 0.01$, ***$p < 0.001$ CON vs. NCoR1 MKO or WT vs. PGC-1α mTg.

Fig. S4

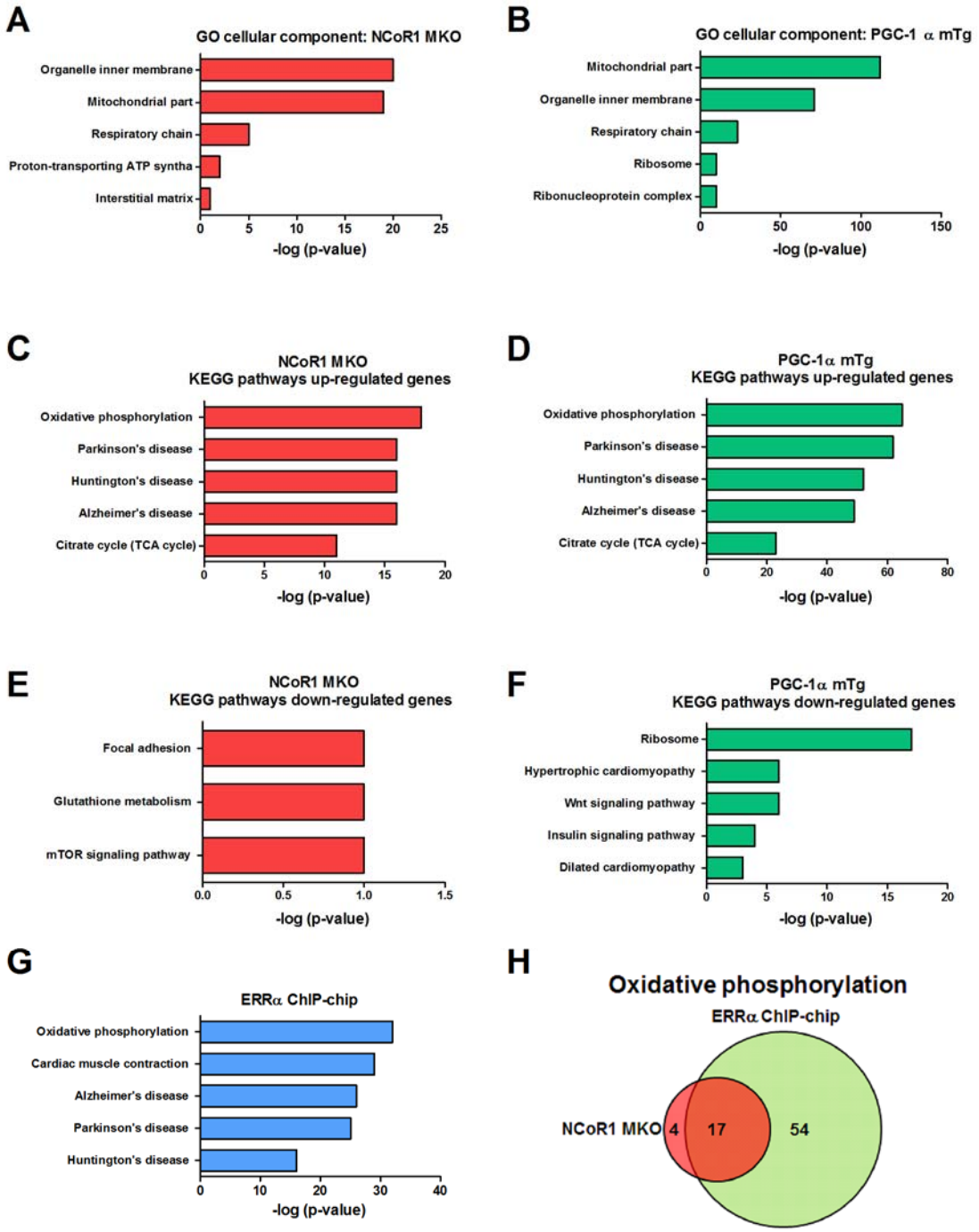

FIG S4 NCoR1 MKO mice exhibit enhanced oxidative metabolism. (*A* and *B*) Top 5 cellular component from GO analysis of the up- and down-regulated genes from the NCoR1 MKO and PGC-1α mTg microarray data sets (n = 5 per group). (*C-F*) Independent GO analyses of

the up- and down-regulated genes from the NCoR1 MKO and PGC-1α mTg microarray data sets (n = 5 per group). (G) Top 5 KEGG pathways from GO analysis of the ERRα ChIP-chip data set (see reference #12 in the main text). (H) Venn diagrams showing the overlap between NCoR1 MKO microarray and ERRα ChIP-chip data set for the genes present in the GO terms “oxidative phosphorylation”.

Fig. S5

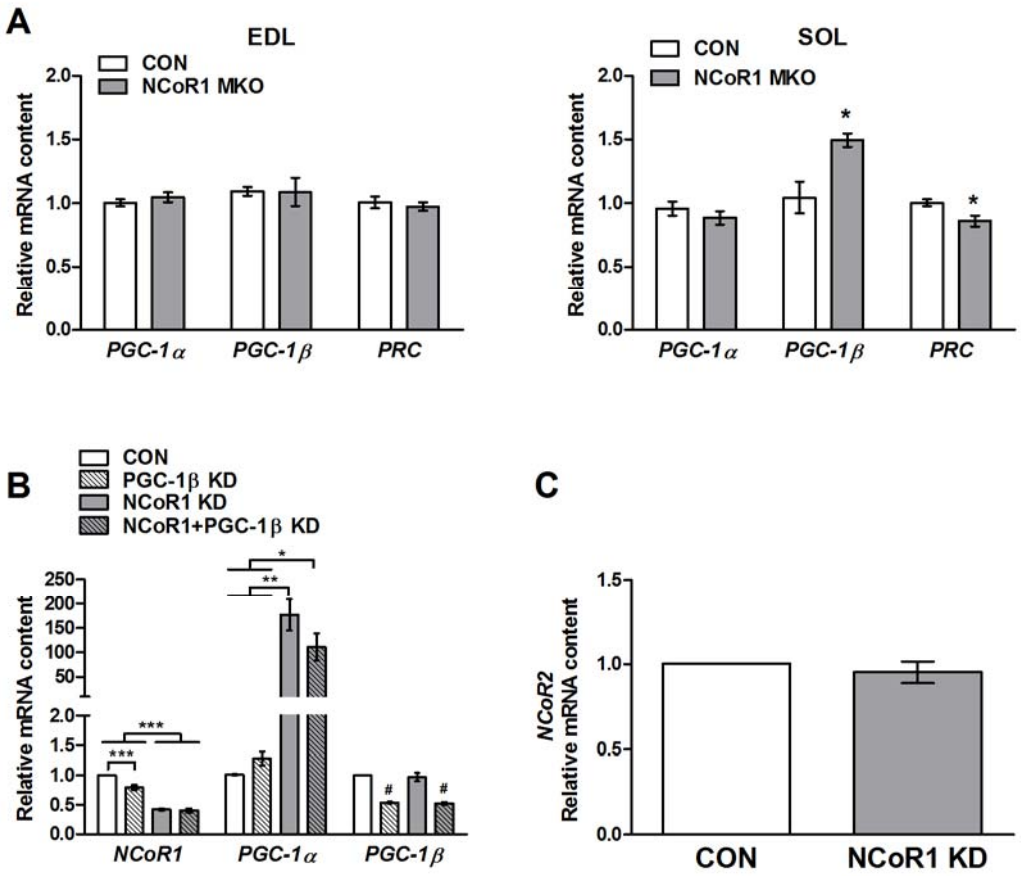

FIG S5 Role of PGC-1α and PGC-1β in NCoR1 modulation of oxidative metabolism. (A) Extensor digitorum longus (EDL) and soleus (SOL) mRNA levels of PGC-1 family of coactivators (n = 7 CON and n = 5 NCoR1 MKO). (B) NCoR1 and LacZ (CON) knockdown (KD) alone or in combination with PGC-1β KD for 48 h in C_2C_{12} myotubes (n = 3 independent experiments performed in triplicate each). (C) NCoR2 mRNA level in C_2C_{12} myotubes transfected with LacZ (CON) or NCoR1 shRNA adenovirus (NCoR1 KD; n = 3 independent experiments performed in triplicate each). Values represent mean ± SEM. *p < 0.05, **p < 0.01, ***p < 0.001 CON vs. NCoR1 MKO or as indicated; $^{\#}p < 0.001$ vs. CON and NCoR1 KD.

Fig. S6

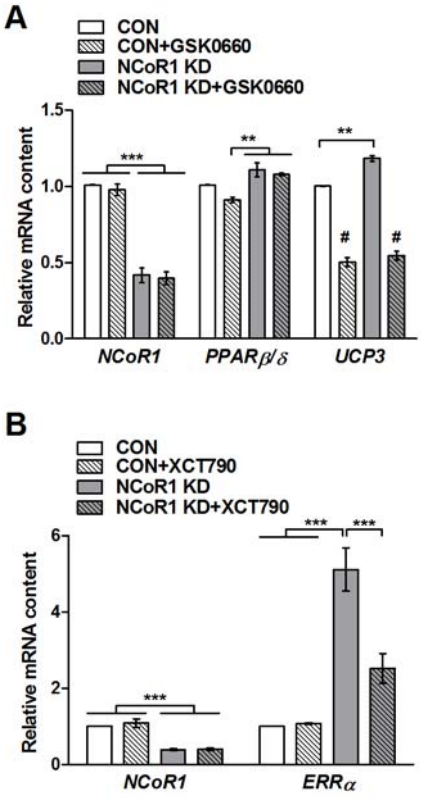

FIG S6 Role of ERRα and PPARδ in NCoR1 modulation of oxidative metabolism. (A and B) NCoR1 knockdown (KD) alone or in combination with 1 µM GSK0660 or 10 µM XCT790 for 48 h in C_2C_{12} myotubes (n = 3 independent experiments performed in triplicate each). Values represent mean ± SEM. $^{**}p < 0.01$, $^{***}p < 0.001$.

Table S1 In vivo and ex vivo assessment of muscle function

In vivo: exercise performance	Maximal test		Endurance test	
	CON	NCoR1 MKO	CON	NCoR1 MKO
Speed (m/min)	17.8 ± 1.2	19 ± 0.4	13.5 ± 7	14.4 ± 0.5
Distance (m)	219 ± 28	248 ± 15	556 ± 160	561 ± 45
Time (sec)	1013 ± 96	1120 ± 48	2778 ± 674	2789 ± 190
Work (W)	449 ± 67	494 ± 26	979 ± 294	972 ± 100
Power (J)	0.42 ± 0.03	0.44 ± 0.01	0.32 ± 0.02	0.35 ± 0.01
Ex vivo: contractile kinetics	**EDL**		**Soleus**	
	CON	NCoR1 MKO	CON	NCoR1 MKO
Twitch				
Time to peak (ms)	12.6 ± 0.9	11.3 ± 0.3	21.4 ± 0.8	23.0 ± 1.2
Half time to peak (ms)	3.5 ± 0.2	3.2 ± 0.0	5.6 ± 0.3	5.9 ± 0.3
Half relaxation time (ms)	18.5 ± 1.9	16.4 ± 0.5	38.5 ± 2.1	32.1 ± 2.3
Tetanus				
Half contraction time (ms)	22.1 ± 1.4	20.8 ± 1.3	35.9 ± 2.4	34.3 ± 2.6
Half relaxation time (ms)	24.7 ± 1.6	21.8 ± 1.4	58.6 ± 2.0	53.3 ± 2.8

In vivo: n = 8 CON and n = 7 NCoR1 MKO mice; Ex vivo: n = 10 CON and n = 14 NCoR1 MKO muscles. Values represent mean ± SEM.

Table S2 MARA prediction of motifs with increased and decreased activity in NCoR1 MKO and PGC-1α mTg skeletal muscle (n = 5 per group)

NCoR1 MKO	
Motif with increased activity	**z-value**
ESR1.p2	2.40
RXR{A,B,G}.p2	2.29
RXRA_VDR{dimer}.p2	2.26
ESRRA.p2	1.85
FOXO1,3,4.p2	1.79
RXRG_dimer.p3	1.68
EVI1.p2	1.62
ELF1,2,4.p2	1.57
NFE2.p2	1.51
Motif with decreased activity	**z-value**
NKX6-1,2.p2	-3.41
ZFP161.p2	-3.10
FOXA2.p3	-2.82
ZBTB6.p2	-2.26
MAFB.p2	-2.10
DBP.p2	-1.74
ZBTB16.p2	-1.57
PGC-1α mTg	
Motif with increased activity	**z-value**
RXR{A,B,G}.p2	10.12
ESRRA.p2	9.14
ESR1.p2	7.52
NR5A1,2.p2	7.35
RXRA_VDR{dimer}.p2	4.61
IKZF1.p2	3.08
FEV.p2	2.83
ZNF148.p2	2.40
HNF4A_NR2F1,2.p2	2.36
SPZ1.p2	2.28
NFE2L1.p2	2.17
CTCF.p2	2.01
POU3F1..4.p2	1.95
SPIB.p2	1.94
NANOG.p2	1.75
HMX1.p2	1.73
ONECUT1,2.p2	1.73
POU6F1.p2	1.67
ZEB1.p2	1.65
ZNF238.p2	1.61
FOXO1,3,4.p2	1.60
bHLH_family.p2	1.59
FOXP3.p2	1.57
NHLH1,2.p2	1.57
Motif with decreased activity	**z-value**
TFDP1.p2	-5.83
MZF1.p2	-4.66
ARNT_ARNT2_BHLHB2_MAX_MYC_USF1.p2	-4.35
EGR1..3.p2	-3.91
EOMES.p2	-3.88
MYBL2.p2	-3.87
POU5F1.p2	-3.64
MAZ.p2	-3.43
PAX2.p2	-3.23

ZBTB6.p2	-3.22
MYB.p2	-3.19
MEF2{A,B,C,D}.p2	-2.89
YY1.p2	-2.72
GLI1..3.p2	-2.72
EHF.p2	-2.70
RFX1..5_RFXANK_RFXAP.p2	-2.44
TLX2.p2	-2.31
XBP1.p3	-2.31
NFATC1..3.p2	-2.20
ZIC1..3.p2	-2.18
NKX3-2.p2	-2.18
GATA1..3.p2	-2.11
ATF5_CREB3.p2	-2.02
TFAP2B.p2	-2.01
HOX{A4,D4}.p2	-1.95
HOX{A6,A7,B6,B7}.p2	-1.86
STAT5{A,B}.p2	-1.82
BPTF.p2	-1.80
HBP1_HMGB_SSRP1_UBTF.p2	-1.79
HSF1,2.p2	-1.77
GFI1B.p2	-1.76
ELK1,4_GABP{A,B1}.p3	-1.71
FOXN1.p2	-1.69
MAFB.p2	-1.69
CEBPA,B_DDIT3.p2	-1.67
RBPJ.p2	-1.63
FOS_FOS{B,L1}_JUN{B,D}.p2	-1.59
ATF6.p2	-1.58
PITX1..3.p2	-1.55
NFE2L2.p2	-1.52
NRF1.p2	-1.50

Table S3 Real-Time PCR primer list.

Target gene	Forward primer	Reverse primer
Ncor1	GACCCGAGGGAAGACTACCATT	ATCCTTGTCCGAGGCAATTTG
Ncor2	CCTTCCGTGAGAAGTTTATGCA	CACACTCAGCGACCGTCTTTC
Ppargc1a	TGATGTGAATGACTTGGATACAGACA	GCTCATTGTTGTACTGGTTGGATATG
Ppargc1b	CCATGCTGTTGATGTTCCAC	GACGACTGACAGCACTTGGA
Pparc1	CACCCTGCCGGAGTGAAAT	CGCATTGACTGCTGCTTGTC
Rxra	AACCCCAGCTCACCAAATGACC	AACAGGACAATGGCTCGCAGG
Rxrb	GCCAAGCTGCTGTTACGTCTT	ACAGGTGCTCCAGACACTTGAG
Rxrg	CCGCTGCCAGTACTGTCG	ACCTGGTCCTCCAAGGTGAG
Ppara	GCGTACGGCAATGGCTTTAT	ACAGAACGGCTTCCTCAGGTT
Ppard	GCAAGCCCTTCAGTGACATCA	CCAGCGCATTGAACTTGACA
Pparg	CCCACCAACTTCGGAATCAG	AATGCGAGTGGTCTTCCATCA
Esrra	CGGTGTGGCATCCTGTGA	CTCCCCTGGATGGTCCTCTT
Esrrb	CCCTGACCACTCTCTGTGAATTG	TGGCCCAGTTGATGAGGAA
Esrrg	GCCCAGCCACGAATGAAT	GCAGGCCTGGCAGGATTT
Tfam	GGTCGCATCCCCTCGTCTA	GGATAGCTACCCATGCTGGAAA
Sdha	GCTGGTGTGGATGTCACTAAGG	CCCACCCATGTTGTAATGCA
Ndufa5	ACATGCAGCCTATAGAAAATACACAGA	TCCGCCTTGACCATATCCA
Ndufb5	TTTTCTCACGCGGAGCTTTC	TGCCATGGTCCCCACTGT
Ndufv1	CTTCCCCACTGGCCTCAA	ATACTTGGGCCTGCCATCTG
Fh1	TGCTCTCAGTGCAAAATCCAA	CGTGTGAGTTCGCCCAATT
Sucla2	CGCCACAGTCCAGCAAGTAA	AGCCTGCACCTTTTTATCTGAAGT
Slc25a20	CTGCGCCCATCATTGGA	CAGACCAAACCCAAAGAAGCA
Ucp3	TTTTGCGGACCTCCTCACTT	TGGATCTGCAGACGGACCTT
Pdk4	AAAATTTCCAGGCCAACCAA	CGAAGAGCATGTGGTGAAGGT
Lpl	GGGAGTTTGGCTCCAGAGTTT	TGTGTCTTCAGGGGTCCTTAG
Cpt1b	ATCATGTATCGCCGCAAACT	CCATCTGGTAGGAGCACATGG
Scd2	CGCCGTGGCTTCTTTTTC	CGGGTGTTTGCGCACAA
COX1	TGCTAGCCGCAGGCATTACT	GCGGGATCAAAGAAAGTTGTG
ATP6	ACTATGAGCTGGAGCCGTAATTACA	TGGAAGGAAGTGGGCAAGTG
ND1	TCTGCCAGCCTGACCCATA	GGGCCCGGTTTGTTTCTG
Tbp	TGCTGTTGGTGATTGTTGGT	CTGGCTTGTGTGGGAAAGAT